Advances in Aircraft and Spacecraft Science, *Vol. 4, No. 2 (2017) 93-124*
DOI: http://dx.doi.org/10.12989/aas.2017.4.2.093

Aeroelastic tailoring using crenellated skins –modelling and experiment

Guillaume Francois*, Jonathan E. Cooper[a] and Paul M. Weaver[b]

Department of Aerospace Engineering, University of Bristol, BS8 1TR, U.K.

(Received October 30, 2015, Revised February 17, 2016, Accepted March 8, 2016)

Abstract. Aeroelastic performance controls wing shape in flight and its behaviour under manoeuvre and gust loads. Controlling the wing's aeroelastic performance can therefore offer weight and fuel savings. In this paper, the rib orientation and the crenellated skin concept are used to control wing deformation under aerodynamic load. The impact of varying the rib/crenellation orientation, the crenellation width and thickness on the tip twist, tip displacement, natural frequencies, flutter speed and gust response are investigated. Various wind-off and wind-on loads are considered through Finite Element modelling and experiments, using wings manufactured through polyamide laser sintering. It is shown that it is possible to influence the aeroelastic behaviour using the rib and crenellation orientation, e.g., flutter speed increased by up to 14.2% and gust loads alleviated by up to 6.4%. A reasonable comparison between numerical and experimental results was found.

Keywords: aeroelastic tailoring; aeroelasticity; structural dynamics

1. Introduction

In the next two decades, the airline industry is expected to grow by 5% (Airbus 2013) per annum. Such expansion raises numerous challenges to the aircraft manufacturers, among which the industry's dependency on fossil fuel is one of the biggest. This reliance creates two problems for the industry. First, airline fuel prices have been rising over the past decade and are projected to continue with this trend. For example, in 2003 fuel cost represented only 15% of an airline overall cost; in 2013 this figure has doubled to 30% (Airbus 2013). Rising costs for airlines directly threaten their growth. Secondly, the growing problem of fuel consumption and its impact on the environment is a major concern.

To remedy these problems, aircraft manufacturers have traditionally improved the engine fuel efficiency and reduced weight where possible. Unfortunately, this source of improvement is decreasing and is forcing aircraft designers to find efficiency savings by reducing aircraft weight and drag. These considerations require future aircraft to be optimized and designed with new concepts that offer advantages over traditional ones.

*Corresponding author, Ph.D. Student, E-mail: guillaume.francois@bristol.ac.uk
[a]Professor, E-mail: j.e.cooper@bristol.ac.uk
[b]Professor, E-mail: paul.weaver@bristol.ac.uk

Copyright © 2017 Techno-Press, Ltd.
http://www.techno-press.org/?journal=aas&subpage=7 ISSN: 2287-528X (Print), 2287-5271 (Online)

The tailoring of aeroelastic performance is increasingly considered by aircraft designers as a means to reduce aircraft weight and optimize the aeroelastic shape throughout flight, thereby increasing overall efficiency. Understanding the different methods by which aeroelastic performance can be tailored is, therefore, important to aircraft designers. Initial work in this area has considered tailoring the lay-up of the composite skins to impact the bend-twist coupling of the wing. This effect was achieved through optimization of the stacking sequence (Eastep *et al.* 1999, Guo *et al.* 2011, Guo 2007, Kim and Hwang 2005, Manan *et al.* 2010, Weisshaar 1981, 1987) and/or the development of novel manufacturing techniques (Jutte *et al.* 2014, Stanford *et al.* 2015, Stodieck *et al.* 2013, 2014).

Recently, work has focused on the use of tailored internal wing structures to change the bend-twist coupling of the wing. Interestingly, novel structural concepts to control aeroelastic tailoring have been found through the use of optimization methods and can thus be split between the two main methods used: (1) topology optimization and (2) shape optimization.

Finding the optimal number and shape of structural features is the aim of topology optimization (Bendsøe and Sigmund 2003). Research work using the Solid Isotropic Material with Penalization (SIMP) (Maute and Allen 2004) method or the Level Set (Brampton *et al.* 2012, Dunning *et al.* 2014, 2015) method have shown that significant improvement in aeroelastic tailoring can be achieved through the development of novel wing structure. In addition, Kolonay and Kobayashi (2010) showed similar improvements in aeroelastic tailoring using a cellular division method to perform topology, shape and sizing optimization of a fighter aircraft wing box. However, aeroelastic tailoring achieved through topology optimization often discards conventional structural members such as spars, ribs and stringers and generates complex solutions often hard to transfer into real designs.

Shape optimization focuses on finding the most advantageous structural members shape and arrangement for wing box composed of conventional structural members such as spars, ribs and stringers. The use of variable angles between the spars and the ribs to modify the bend-twist coupling of a wing was first shown by Harmin *et al.* (2011) on an aluminium wing. They proved that the change in bend-twist coupling could increase the flutter speed of a wing. Later, Francois *et al.* (2015) investigated this impact on a set of aerofoil profiled wings in a set of static and dynamic wind-off and wind-on tunnel tests.

When considering structural members shape optimization, Vio and Fitzpatrick (2012), Vio *et al*. (2012), Francois and Cooper (2014) showed that the use of curved spars and ribs can lead to significant increase in flutter/divergence speed and in reducing the root bending moment during a gust encounter. This research applied the concept of curvilinear spars and ribs using fixed nodes attaching the ribs and spars and so using a large design freedom. Locatelli *et al.* (2011), Liu *et al.* (2015, 2014) have used curved spars and ribs to perform wing weight optimization subject to stress, buckling and aeroelastic flutter constraints on complex wing design. In their work the spars and ribs curvatures were decoupled from the rib/spar arrangement. Such an approach was later taken by Jutte *et al.* (2014) to show that aeroelastic properties could be impacted positively by the use of curved spars and ribs. Finally, Francois *et al.* (2014) showed that curved spars and ribs in a reduced design freedom framework resulted in wings with improved flutter speed while meeting buckling and stress constraints for both backward and forward swept wings. Preliminary studies by Harmin *et al.* (2011) on the use of the internal structure on metallic wings for aeroelastic tailoring has shown that improvements in flutter speed can be made through the variation of the skin thickness along the wing - a concept known as crenellated skins as shown schematically in Fig. 1.

In this paper, the use of crenellated skins is further advanced though a series of numerical

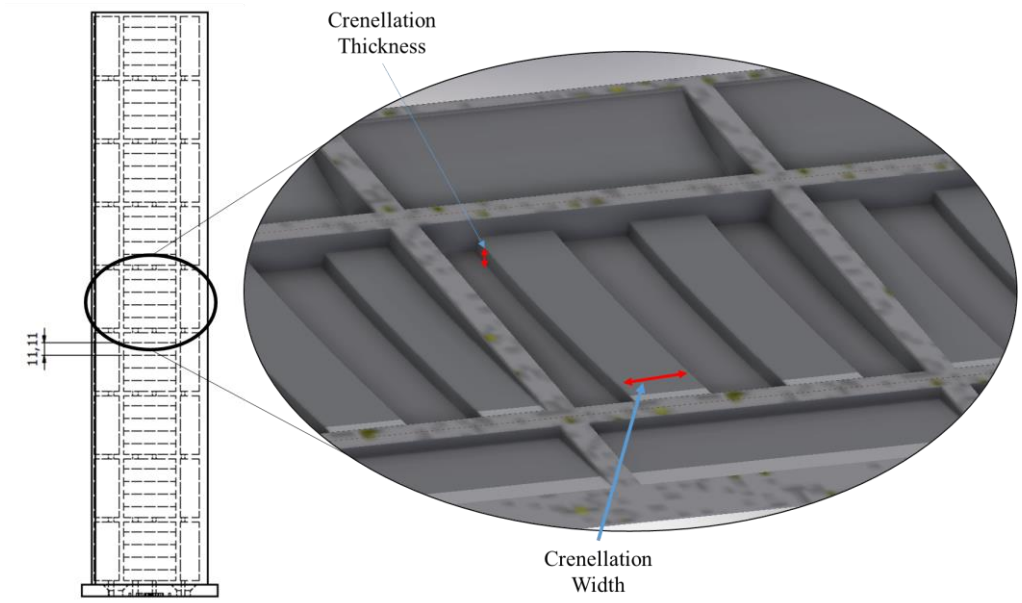

Fig. 1 Illustration of a crenellated skin between the spars on an un-tapered, un-swept wing. Dimensions are in mm

modelling and experimental investigations. The impact of the crenellation angle and crenellation size on the wing's bend-twist, aeroelastic and modal response behaviour, is investigated.

2. Concept & wing model

2.1 Concept

We consider the effect that a crenellated skin has on wing deformation under aerodynamic loads. A crenellated skin is a skin of periodically varying thicknesses in, predominantly, the span-wise direction as shown in Fig. 1. In this paper, the following variables are used to assess the impact of the crenellated skin concept: (1) number of crenellations, (2) thickness of crenellations and (3) orientation of the crenellation with respect to the leading edge spar. Although Harmin *et al.* (2011) showed the impact of the number and the thickness of the crenellation with respect to the orientation with the leading edge spar, a key difference with this work is the combination of crenellation and rib orientation. As such, we consider crenellations and ribs where both have a similar orientation. Additionally, the crenellations are placed only between the two spars. Finally this work attempts to experimentally validate the Finite Element (FE) results.

2.2 Wing model

The wing geometry is untapered and un-swept with a span of 500 mm and a chord of 100 mm. The skin and spar/rib thickness are 2 mm and 4mm respectively. The wing's internal structure consisted of 8 ribs, 2 spars and a root and tip ribs. The leading and trailing edge spar were placed

at 25% and 75% of the wing chord, respectively. So as to avoid an increase in the skin panel size the change in rib/crenellation orientation created a half rib at each end of the wing. It should be noted that no crenellations were placed between the half rib and the tip/root rib introduced when the rib/orientation changed from the stream-wise position. Hence changing the rib/crenellation orientation away from the stream-wise position moved the first crenellation away from the root (in contact to the half-rib at the root). Additionally, the introduction of crenellations on the skin did not move the position of the ribs - the rib spacing was maintained constant at the mid-chord position (56.56 mm). Finally, it should be noticed that no attempt to balance the mass increase due the addition of crenellations/ribs was made, in this work as opposed to work done by Harmin *et al*. (2011), because of manufacturing tolerances.

Two different wing models were used: (1) a wing with a NACA 0012 aerofoil profile and of constant thicknesses for the spars and ribs and (2) a rectangular wing box with a constant thickness to chord ratio of 9.5% and of constant thicknesses for the spars and ribs. The constant thickness to chord ratio of the rectangular wing box was approximated by assuming thin-wall beam theory and considering the second moment of area contribution of the different structural members of the profiled wing section using

$$h = \sqrt{\frac{\sum h_i^2}{n}} \tag{1}$$

where, h is the equivalent rectangular wing box height, h_i is the actual height of element i on the NACA profile wing box and n is the number of element considered. In this case only the two spars were considered as the spars height are the main differences between the rectangular wing box and the profiled wing section.

The dimensions of the different crenellated skins modelled are summarized in Table 1 and apply for all rectangular wing boxes considered in this paper. The first crenellation is always after the root rib in the case of the 0° rib/crenellation orientation and after the root half rib in all other cases.

NACA profiled wing were made with no crenellations and crenellations with width 11.11 mm and thickness of 4 mm to match experimentally tested wings. For the wing with crenellation width of 11.11 mm and 0° rib/crenellation orientation, a slight difference existed in the order between the

Table 1 Dimensions of crenellations modelled

Crenellation Width (mm)	Total Number of Crenellations	Number of Crenellations per rib bay	Thickness Increase due to Crenellations	Thickness of Skin at the Crenellations (mm)
6.17	41	4-5	2	4
7.94	32	3-4	2	4
11.11	23	2-3	1.5	3
11.11	23	2-3	2	4
11.11	23	2-3	2.5	5
18.52	14	1-2	2	4
27.78	9	1	2	4

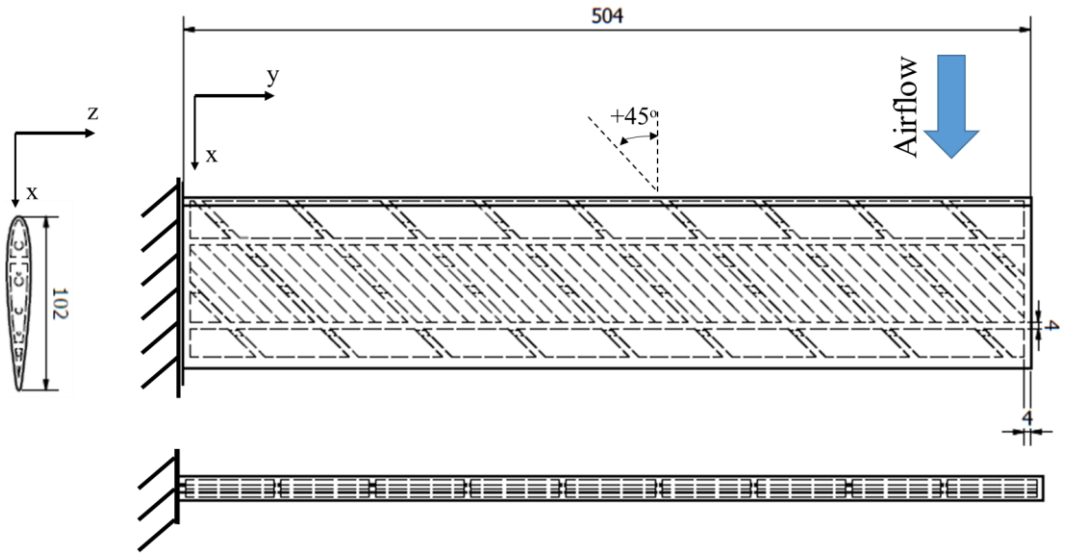

Fig. 2 Wing model external dimensions in mm, rib/crenellation orientation and axis convention

NACA profiled wing and the rectangular wing box. The NACA profiled wing has a normal skin thickness region after the root rib instead of a crenellation; hence that wing has one less crenellation on the whole wing than its rectangular counterpart. These changes were done to match the manufactured wing.

For the experimental part of this research only the aerofoil profiled wing model was used. The rib/crenellation orientation is indicated with respect to the incoming air flow and a positive orientation means the rib/crenellation leading edge are pointing towards the root. The wing dimensions and the rib/crenellation orientation sign convention are shown on Fig. 2.

3. Wing structural modelling & manufacturing

3.1 Wing structural modelling

Modelling of the different wing designs considered was performed using Finite Element (FE) analysis. The geometry and the actions needed to create the different wing models were specified in a MSC.PATRAN session file by a MATLAB script. This session file was then read by MSC.PATRAN. Actions include the creation of the surfaces, meshing of the surfaces, node equivalence and check of the element geometries as well as the creation of element properties and boundary conditions to be used in the different analyses. IsoMesh and the Paver meshing algorithm were used to mesh the wing models. The structural model was made using 2D shell elements. Initially, quadrilateral shell elements (CQUAD4) were used; however, these were replaced by triangular shell elements (CTRIA3) if the skew angle of the CQUAD4 elements was less than 30° using the MSC.PATRAN mesh verification tool. It should be noted that in the case of the NACA profiled wing, the FE model made no simplification about the wing geometry, and so the curvature of the NACA aerofoil were fully considered and so required a high number of

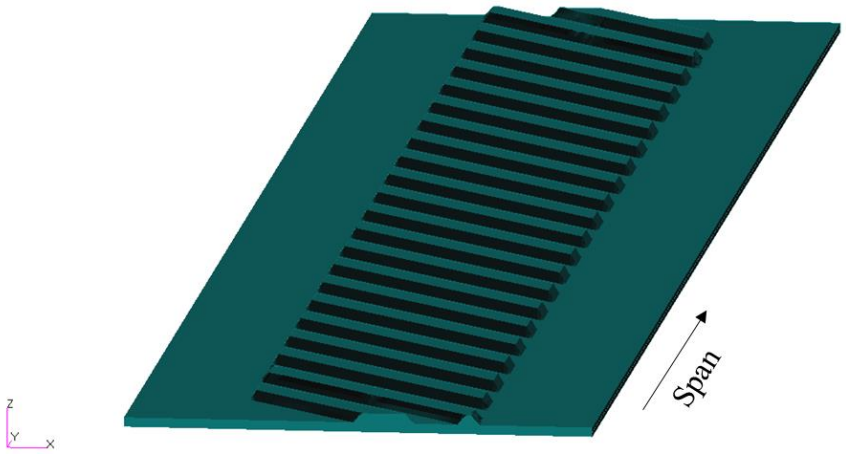

Fig. 3 FE model of a crenellated skin displaying shell thicknesses for a rectangular wing box

Table 2 Cured polyamide material properties as specified by manufacturer

Young's Modulus (N/mm^2)	1,650.0
Flexural Modulus (N/mm^2)	1,500.0
υ	0.4
ρ (kg/m^3)	1,150.0

elements. The NACA profiled FE model mesh contained over 120,000 structural elements and 900 aerodynamic panels for the aeroelastic calculations. The rectangular wing box models used contained over 50,000 structural elements. The mesh convergence of the different models used was checked for the different structural performance of interest.

The FE wing models created using MSC.PATRAN had covers of constant thickness. The variation in thickness needed to model a crenellated skin was implemented though a MATLAB script. The orientation of the thickness axis (z axis) for every element was verified to be similar for all elements in MSC.PATRAN. The increase in skin thickness and a change in offset values for the 2D shell elements on the top and bottom skin making the thick region of the crenellation were made using a MATLAB script and ensured that the crenellations were inside the wing box and that the outside skin was flat as can be seen on Fig. 3.

3.2 Wing manufacturing

The wings used in this paper were laser sintered polyamide as this manufacturing method is cost effective, quick and can accommodate the design freedoms required. The material properties of cured polyamide are reported in Table 2 as specified by the wing manufacturer. So as to validate the Young's modulus value a tensile test was performed with a dog bone specimen (type V) according to ASTM D638-10. The test was carried out using an Instron 3343 electromechanical single column test machine fitted with an Instron 1kN S-beam static load cell with an accuracy of 0.5% of the indicated load. Two different thicknesses were used in this test to assess the impact of component thickness on the material properties. These specimens were also distinguished between painted and non-painted specimens to assess the impact of paint on the wing. An Imetrum video

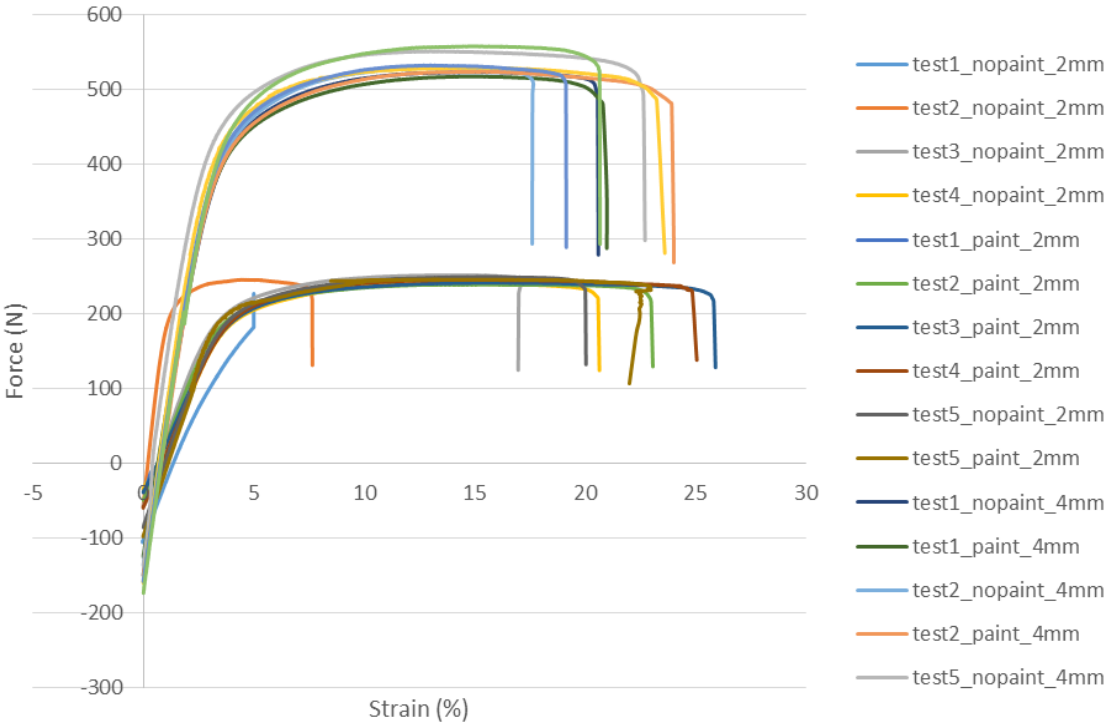

Fig. 4 Tensile test force vs strain for 2 mm and 4 mm thickness specimen

Table 3 Average Young's modulus values, percentage difference with the manufacturer data and standard deviation

	Painted Specimen	Un-Painted Specimen	2 mm Specimen	4 mm Specimen
Average Young's Modulus (N/mm^2)	1392.5	1386.6	1268.9	1500.3
Average % Difference With Manufacturer Data	-15.6	-16.0	-23.1	-9.1
Standard Deviation (N/mm^2)	156.3	179.0	148.9	96.5

gauge system (Imetrum 2016) was used to measure strain of the specimen with an accuracy of 0.01 mm. The results of the tensile test are shown in Fig. 4 and Table 3.

The results show that the paint has little effect on the Young's modulus however the thickness of the specimen does. Thicker specimens have more reliable material properties. To confirm this result a three-point bend test was performed with specimens of 2 mm and 4mm depth according to ASTM D790-10 standard. Force-displacements curves for this test are presented in Fig. 5 and flexural modulus data are presented in Table 4. These values confirm this finding as the 4 mm specimen curves show less scatter than the 2 mm specimen curves.

Finally, a stress relaxation test was carried out. The test consists in maintaining a constant displacement of 1mm on a 4mm specimen over time. Load reduction over time is shown in Fig. 6 and clearly highlights that the polymer undergoes some stress relaxation.

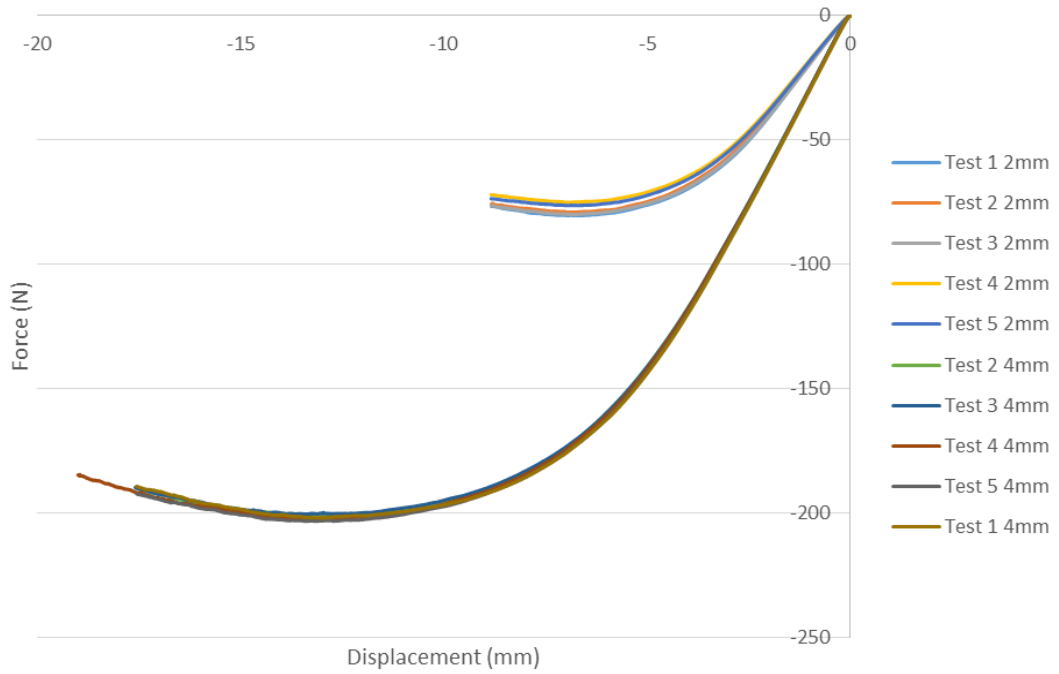

Fig. 5 3 point bend test force vs displacement for 2 mm and 4 mm thickness specimen

Table 4 Average flexural modulus values, percentage difference with the manufacturer data and standard deviation

	2 mm Specimen	4 mm Specimen
Average Flexural Modulus (N/mm^2)	1433.0	1795.6
Average % Difference With Manufacturing Data	-4.5	19.7
Standard Deviation (N/mm^2)	50.7	25.6

Thus it was decided to manufacture six wings with 4 mm thick spar and ribs and 2 mm thick skin. The six wings are: (1) four wings with no crenellation and ribs with an angle of 0°, 30°, 40° and 45° to the inflow and (2) two wings with crenellation of 11mm in width and 2 mm in thickness and ribs/crenellations at an angle of 0° and 45° to the inflow. The wing with crenellations and rib/crenellation at 45° had a total of 23 crenellations. Hence every rib bay had two (or three) regions of standard skin thickness of 2 mm and three (or two) crenellations with a skin thickness of 4mm as shown Fig. 2. The exact number for a particular rib bay was dependent on the location of the rib e.g., the first rib bay has two regions of standard skin thickness and three crenellations while the second rib bay has three regions of standard skin thickness and two crenellations. The first crenellation was after the root half-rib. A manufacturing error meant that the wing with crenellations and rib/crenellation at 0° had a total of 22 crenellations as the region after the root was of standard thickness. Hence every rib bay of that wing had three/two regions of standard skin thickness of 2 mm and two/three crenellations with a skin thickness of 4mm as shown Fig. 1 (e.g., the first rib bay has three regions of standard skin thickness and two crenellations while the second rib bay has two regions of standard skin thickness and three crenellations).

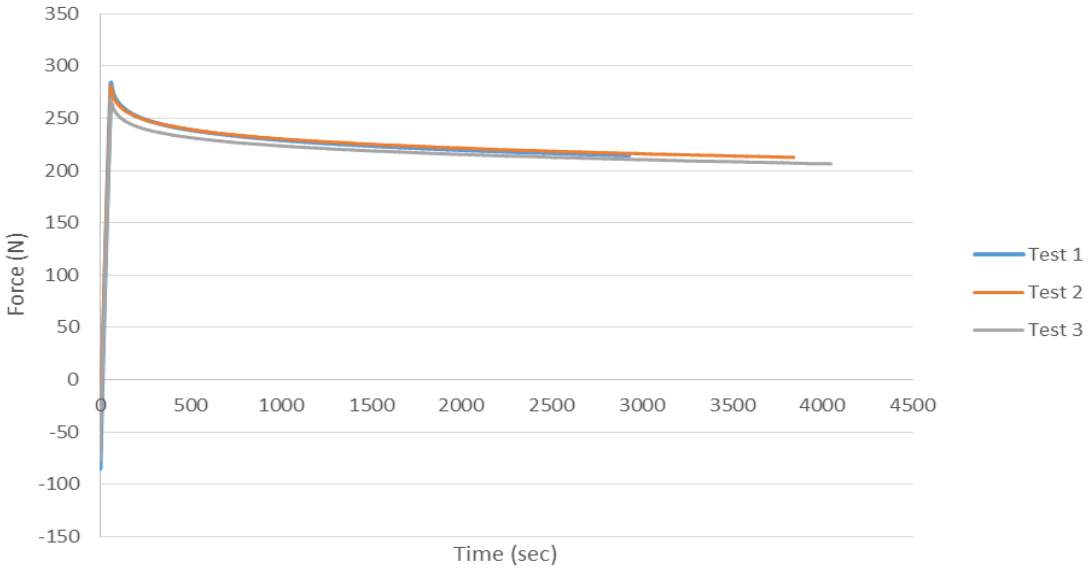

Fig. 6 Force versus time illustrating stress relaxation when specimen are hold at a displacement of 1 mm

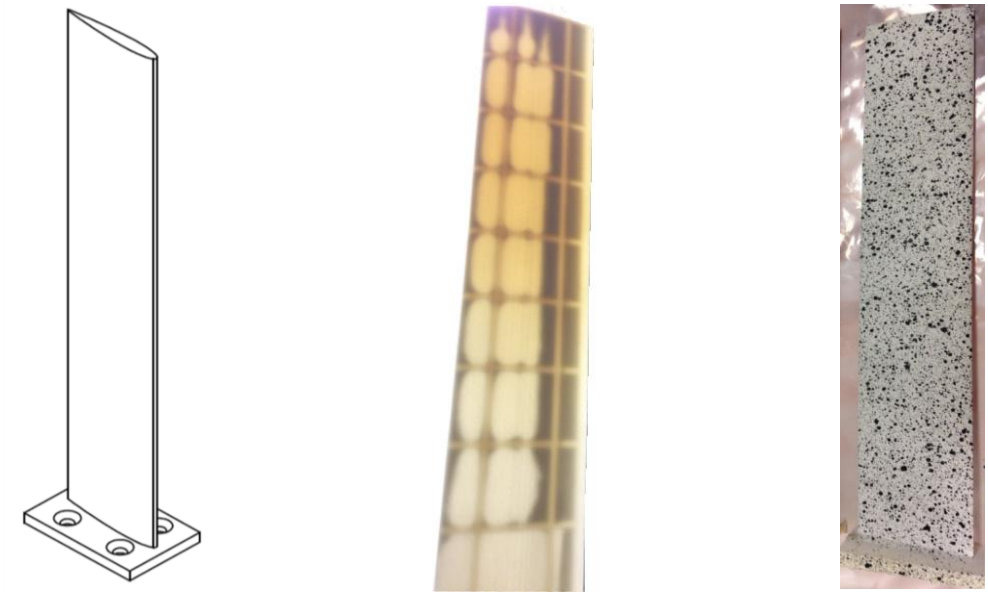

(a) CAD file sent to the manufacturer

(b) View of the excess powder trapped in the wing

(c) Digital image correlation paint pattern on a wing

Fig. 7 Illustration of the wing manufacturing process

The wings were ordered in two batches: the first batch was made of wings with rib/crenellation at orientation 30°, 40° and 45° and the second batch contained wings with rib/crenellation of 0°. The same printing direction was used for both batches. The fact that the wings were ordered in two batches is a source of material variability.

Table 5 Mass of the wings without and with paint

	Mass - No Paint (g)	Mass - With Paint (g)
Ribs @ 0°	320	327
Ribs @ 30°	350	355
Ribs @ 40°	361	369
Ribs @ 45°	370	376
Ribs and Crenellations @ 0°	390	399
Ribs and Crenellations @ 45°	417	422

A rectangular root section was manufactured with each wing, as shown in Fig. 7, to permit the fixation of the wings to the bench/wind tunnel. Four small holes were placed in the ribs to remove excess powder trapped after manufacturing. A small amount of powder remained trapped in the wings as can be seen by the dark areas on Fig. 7. Finally, two coats of white paint were applied on both sides and black paint speckles were applied on one side of the wings as shown by Fig. 7 to enable the use of Digital Image Correlation (DIC). The variation in wing mass with and without paint is shown in Table 5.

4. Analysis performed

4.1 Static analysis

To assess the impact of the crenellations on the wing deflection and twist a static analysis (SOL 101) was performed for every wing design considered. The wings were assumed to be fully fixed at the root. A tip load was applied though a Multiple Point Constraint (MPC) slaving all the tip nodes to a node placed at the tip mid chord and at the middle of the wing depth. This loading condition generates a bending load and a torque for an aerofoil profiled wing. All FE analyses was performed using the highest load used during the experiment: 487 g.

The static experiment reproduced the static loading modelled in FE. A series of loads were applied on the wing using the Load Application Device (LAD). The loads were 124, 245 and 487 g. The use of three loads allowed to assure no plastic deformation occurred during the test. The LAD consisted of a rectangular part with an opening of the shape of the wing aerofoil which is slightly larger than the wing aerofoil. The LAD was 1cm thick hence the tip deflection recorded during the experiment was offset by 1 cm in board. The wings were bolted with four 12 mm steel bolts to a bench to assure a fully fixed boundary conditions. A 5M pixel cameras 3D Dantec Q400 Digital Image Correlation (DIC) system - a contactless displacement measurement method - was used to measure wing deflections. The DIC cameras were placed above the wings and recorded the whole of the top side deflections. The set up for the static testing is shown in Fig. 8. For every test point, a DIC image was captured after 10min under load. The experiment was repeated three times for the wings with rib/crenellation orientation of 0° and 30°, and four times for all other wings.

Secondly, the position of the Flexural Axis was estimated for the wing boxes in FE modelling by applying a unit load at the leading and trailing edge at various sections along the wing models. This analysis assumed that the flexural axis is the line connecting flexural centres which are a point on a wing section at which the application of a shear force creates no twist of that section

with respect to the root (Stodieck *et al.* 2015, Tatham 1951).

4.2 Aeroelastic analysis

The static aeroelasticity analysis (MSC.NASTRAN SOL 144) was performed at an angle of attack of 5° and at a speed of 35 m/s using a doublet lattice panel method. The deflection and twist of the wing under different aeroelastic loading was assessed. In this analysis the wing was assumed to be fully fixed at the root. This analysis was applied to both FE models. The modelling was performed at an air temperature of 25℃ similarly to the temperature experienced in the wind tunnel. A symmetry at the root was assumed to consider the reflection from the wind tunnel wall (Rodden and Johnson 1994).

To match the modelling conditions experimentally, the manufactured wings were placed horizontally in the low turbulence wind tunnel at the University of Bristol and fixed to one wall. The DIC camera was placed outside the wind tunnel looking at the underside of the wings through a glass wall to measure the deflection and twist of the wing. Due to distance restrictions only the tip end of the wing was in the field of view of the cameras. The wind tunnel set up is shown in Fig. 8. The wings were fixed at an angle of attacks of 5° and the wind tunnel speed was set at 0, 25, 30 and 35 m/s. At each test point, a DIC image was captured after 2min, 4min and 5min under load. A temperature variation of no more than 2℃ was observed during the tests. The experiment was repeated three times for every wing.

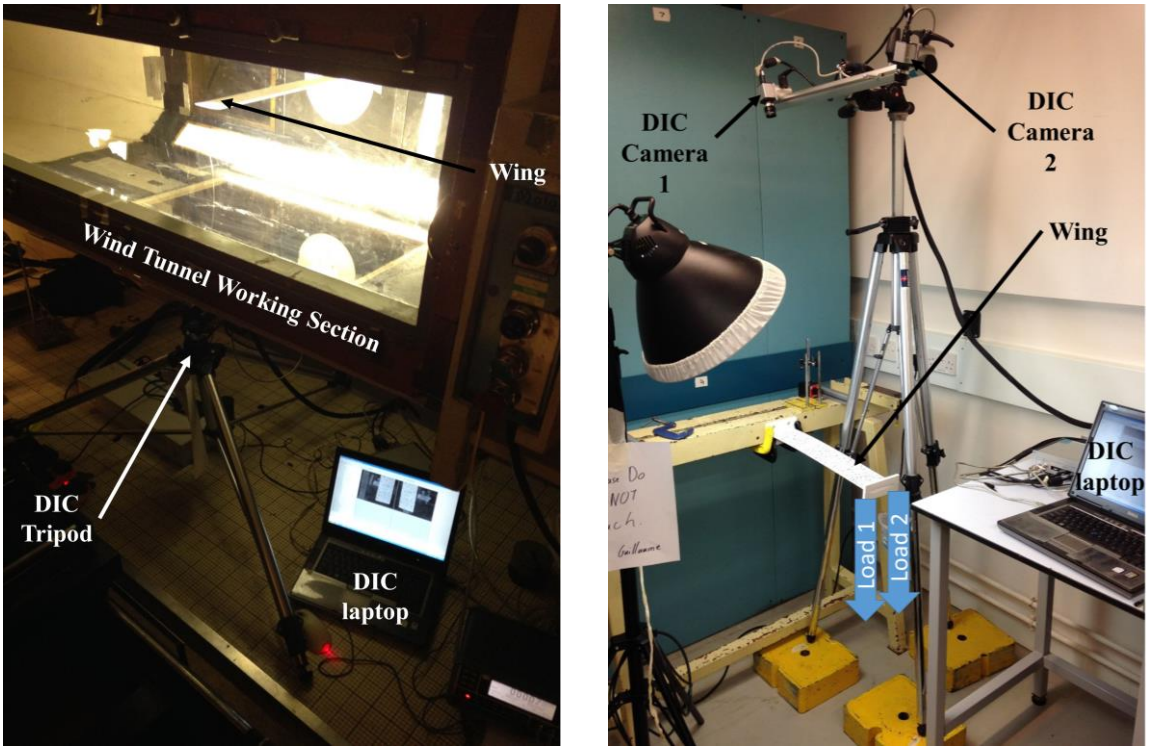

(a) Wind tunnel experimental set-up (b) Static testing experimental set-up

Fig. 8 Experiment set-up

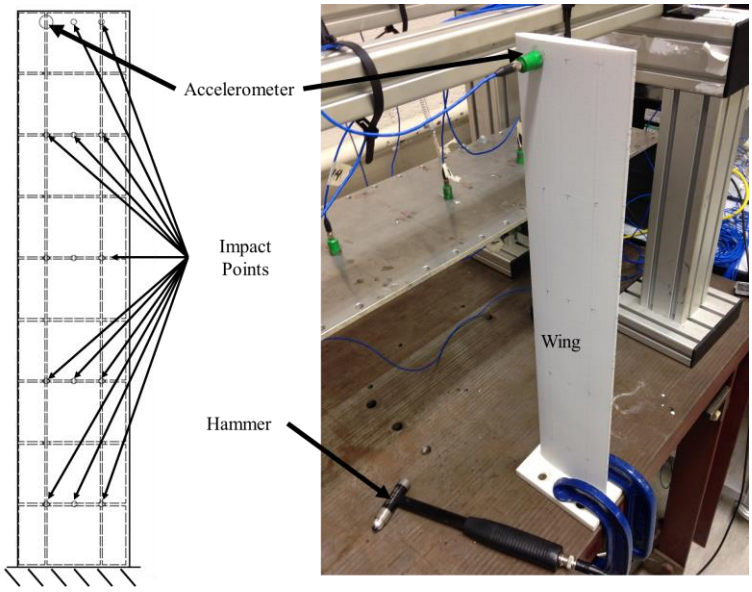

Fig. 9 Accelerometer and impact locations and dynamic experiment set up

4.3 Modal analysis

The natural frequencies of the different mode shape of the wings were estimated using modal analysis (MSC. NASTRAN SOL 103). These results were compared with the experimental ones. The wing was, once again, assumed to be fully fixed at the root.

Dynamic testing was used to find the natural frequencies, damping ratios and the associated mode shapes. A "hammer" test was performed using a single accelerometer placed at the tip of the wing and impacting the structure at various impact points as shown by Fig. 9 using five averages. The data measurement and analysis was performed using LMS International software.

4.4 Gust analysis

Gust loads can be of crucial importance to aircraft designer as they can be the design loads for which the wing structure is sized. It is, therefore, important to assess the impact of the crenellation concept on gust loads. The gust analysis performed assumed a discrete '1-Cosine' gust analysis using MSC.NASTRAN SOL 146 for which the time domain gust velocity was expressed using

$$w_g(t) = \frac{w_{g0}}{2}\left(1 - \cos\frac{2V\pi}{L_g}t\right) \tag{2}$$

with t the analysis time variable, w_g, 0.5 m/s, the peak gust velocity and the gust length L_g (Wright and Cooper 2007). The gust analysis was performed in the frequency domain using a doublet-lattice panel method at sea level at a speed of 35 m/s and at 25℃. The output considered was the root bending moment time history. Since the wing was fully fixed only one gust length of 25 times the mean chord of wing was used (European Aviation Safety Agency 2013). A symmetry at the root was assumed to consider the reflection from the wind tunnel wall (Rodden and Johnson

1994).

The wing is assumed to be fully fixed during the analysis through an MPC at the root. Thus to quantify the load during a gust encounter the root bending moment was assessed by considering the bending moment created on the node salving all the nodes at the root. A value of 0.7% of structural damping was used in this analysis.

4.5 Aeroelastic instability speed analysis

The aeroelastic instability speed analysis was performed using MSC.NASTRAN PKNL analysis (SOL 145). The PKNL method is a PK method that uses direct matching of air speed, Mach number and air density at which to investigate the behaviour of the wing (Johnson 1997, Rodden and Johnson 1994). The analysis was performed with a range of Mach number from 0.01 to 0.5 with matching airspeed at sea level and at 25℃ using a doublet lattice panel method. A symmetry at the root was assumed to consider the reflection from the wind tunnel wall (Rodden and Johnson 1994). The first aeroelastic instability was found by tracking sign inversion in the mode damping values. The inclusion of 0.7% of structural damping prevented the triggering of soft flutter modes in the analysis (Rodden and Johnson 1994, Wright and Cooper 2007).

5. Results

In the following section, the average tip displacement is calculated by averaging the displacement at the leading and trailing edge. Nose up twist is shown by a positive twist value.

5.1 Static analysis

Fig. 10 and Fig. 11 show the average tip displacement and tip twist obtained by FE analysis, for various crenellation widths and rib/crenellation orientations on a rectangular wing box (RWB). First, it can be seen that the change in rib orientation - when no crenellations exist - creates a small variation in tip displacement and alteration in tip twist. The initial reduction in tip displacement with the rib orientation is due to the addition of material to the wing due to the introduction of the half rib at the tip and root and the increase in length of the rib. Then the tip displacement first increases with the increase of rib orientation and then decreases once the rib orientation is above 25°. Above this value the ribs change their structural behaviour and increasingly act as spars - increasing the span-wise stiffness.

Although the variation in tip displacement due to the variation in rib orientation is small it is interesting to note the ability of the rib orientation to change the sign of the tip twist rotation and provide a cubic polynomial curve with two distinct stationary points where similar values of twist can be achieved with different rib orientations as shown by Fig. 11.

The addition of crenellations creates a reduction of at least 3.7% in average tip displacement. This result increases as the crenellation gets wider, as explained by the thicker skin provided by the crenellations which increases the second moment of area of the wing and prevents wing deflection.

Fig. 10 shows that the trends in average tip displacement variation with the rib/crenellation orientation is similar to the one observed with changing just the rib orientation for all the crenellation widths considered except the widest crenellation. For the wings with crenellation

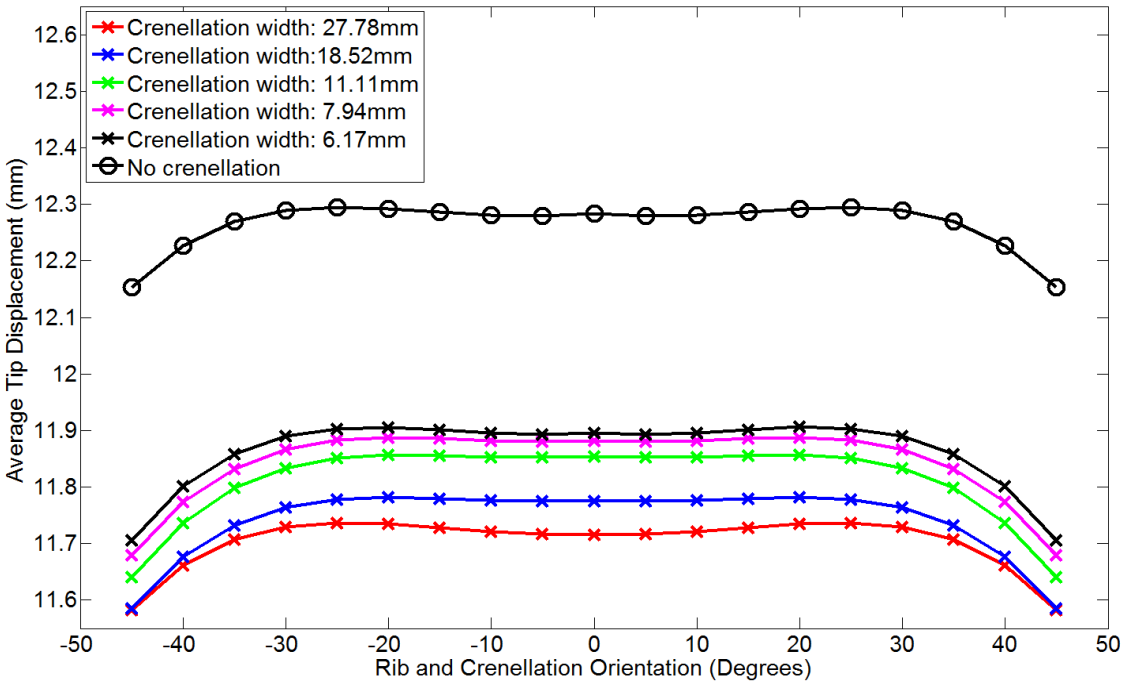

Fig. 10 Average tip displacement for different crenellations width and rib/crenellation orientation on a Rectangular Wing Box (RWB)

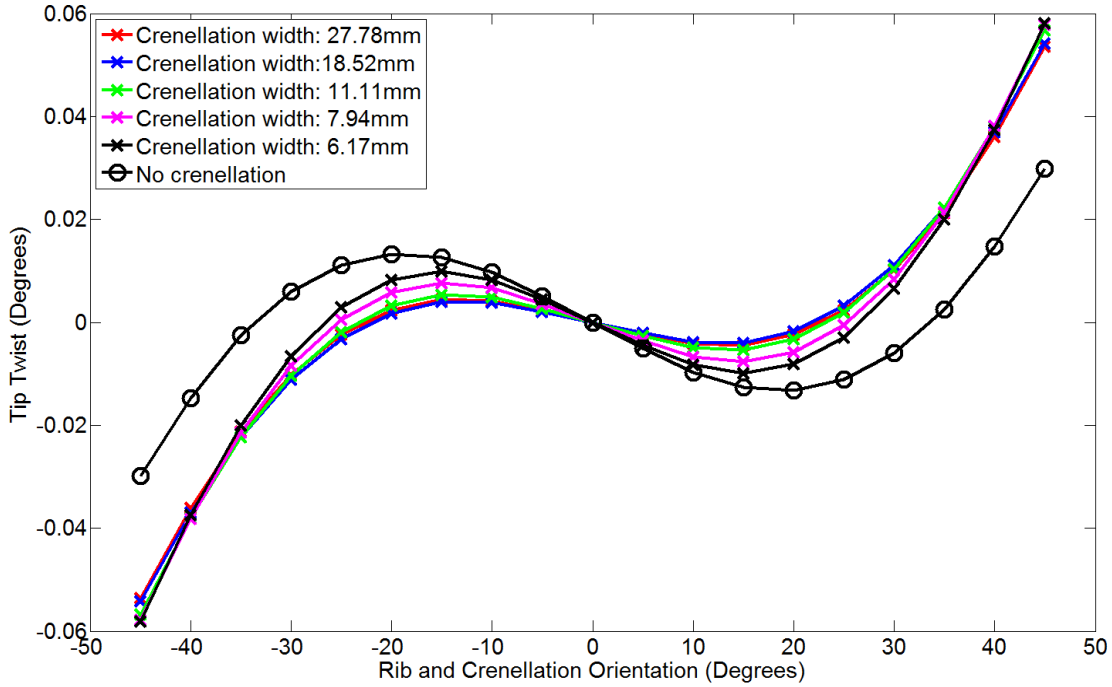

Fig. 11 Tip twist for different crenellations width and rib/crenellation orientation on a Rectangular Wing Box (RWB)

width of 27.78 mm the stiffening effect due to the rib/crenellation orientation is less than the one observed for other crenellations widths. Note that the widest crenellation concept is the only one with an identical number of crenellations for every rib bay as shown by Table 1 hence the centre of gravity of those wings are slightly offset from the mid-span location towards the tip. Thus the increase in material due to the change in rib/orientation does not follow the same pattern as the other concepts and explains the change in average tip displacement versus rib/crenellation orientation's trend.

Interestingly, the addition of crenellation increases the tip twist especially when the crenellations are placed at high orientations. Overall, the addition of crenellation reduces the ordinate distance between the two stationary points of the cubic tip twist curve created by varying the rib orientations.

Fig. 12 and Fig. 13 show the change in average tip displacement and tip twist for various crenellation thicknesses and rib/crenellation orientations. Clearly, when the crenellation thickness is increased the average tip deflection is reduced. This effect can be related to an increased second moment of area. The crenellation thickness has an interesting impact on the tip twist curves. The highest tip twist is achieved at high crenellation orientations and with a crenellation thickness of 4mm and this crenellation thickness also has the tip twist curve with the second lowest ordinate distance between stationary points. While a wing with a crenellation thickness of 5 mm has the second highest twist and yet its tip twist curve is almost similar to the wing with no crenellation in the crenellation orientation range [-10°, 10°].

Fig. 14 and Fig. 15 show the average displacement and twist at 15 mm from the tip for the

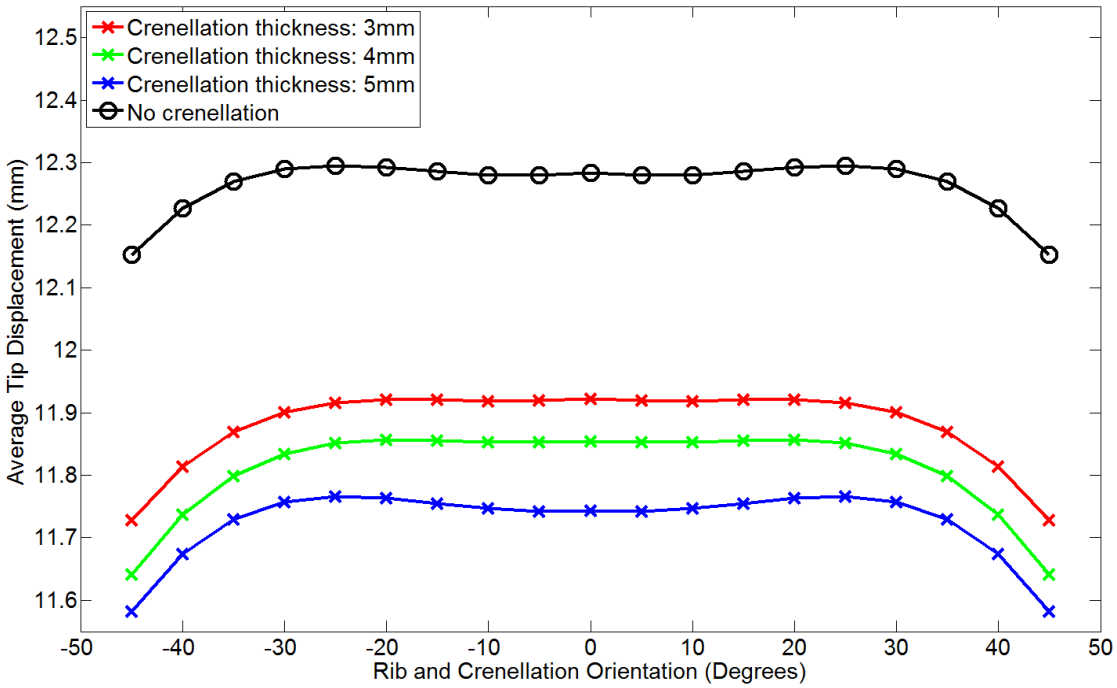

Fig. 12 Average tip displacement for different crenellations thickness and rib/crenellation orientation on a Rectangular Wing Box (RWB)

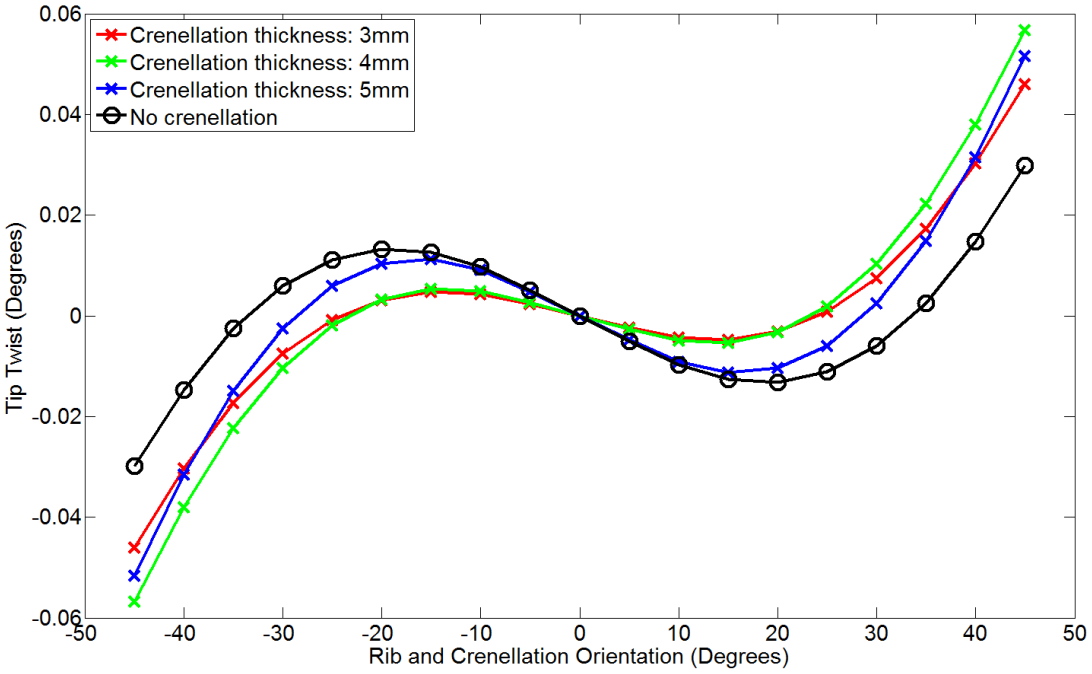

Fig. 13 Tip Twist for different crenellations thickness and rib/crenellation orientation on a Rectangular Wing Box (RWB)

NACA profiled wing box (NWB) with no crenellations and with crenellation widths of 11.11 mm noting that both FE and experimental results are presented. The FE analysis was performed assuming an elastic material with the three different tensile moduli presented in Section 3.2 (1,500 MPa, 1,650 MPa and 1,800 MPa) to illustrate the effect of tensile modulus variation on the tip displacement and twist. The experimental results presented for each wing are the average of at least three experiment runs and the standard deviation for the experimental data is shown as error bars.

First, the FE results show that the impact of changing the rib orientation is highly similar for a rectangular and NACA profiled wing box. A noticeable difference is the lack of symmetry around the 0° rib orientation for the NACA profiled wing box in the average tip displacement and tip twist curves. This result is due to the lack of geometric symmetry about the mid-chord depth plane of the NACA profiled wing box. This implies that a tip load at the mid-chord point has both bending and torsion components, as manifested by the existence of a tip twist in the 0° rib orientation case.

The addition of the crenellation has a similar impact in both the rectangular wing box and the NACA profiled wing box: a reduction in the average tip displacement values and a reduction in the ordinate distance between the two stationary points of the cubic tip twist curve. Once again, the removal of the symmetry in the box depth removes the symmetry in the tip displacement and twist results.

It should be noticed that the difference in crenellation scheme for the wing with crenellations width of 11.11 mm and 0° rib/crenellation between the NACA profiled and the rectangular wing box models explains the slight increase in tip displacement at 0° rib/crenellation orientation displayed by the NACA profiled model.

When considering the variation in rib orientation the trend predicted by FE results was also shown in the experimental results: reduction of the displacement and nose down twist as the rib orientation increases. For example, a variation of the rib orientation form 30° to 45° predicted a reduction in average tip displacement of 2.2% and 1.1% and a reduction in tip twist of 36.7% and 39.9% for the experiment and the FE results with a tensile modulus of 1,650 MPa respectively.

The addition of crenellation at a given rib/crenellation orientation reduced the displacement and reduced the nose down twist in the experimental results as predicted by FE results. The impact of such reductions varies, however, between the FE and the experimental results. For example, for the rib/crenellation at an orientation of 45° the experiment and the FE results (E=1,650 MPa) predicted a reduction in average tip displacement of 9.2% and 6.1%, respectively and a reduction in tip twist of 85.5% and 64.1%, respectively due to the crenellation concept. Indeed in the experimental results, the wing with rib/crenellation at 45° orientation showed a nose-up twist.

Although the major trends observed in the FE results were shown in the experimental results it is apparent that a variation existed between the experimental and FE results. It is believed that some of these variations are due to the material property variability observed in Section 3 and the viscoelastic nature of the material used. To illustrate the effect of material variability, stress relaxation and load history in an experiment where the load is not deformation dependent a reduction in the tensile modulus should reduce the error between the FE and experimental results. As shown by Fig. 14 and Fig. 15, the agreement between the FE and experimental results improves when a tensile modulus of 1,500MPa is used in the FE analysis. The maximum error in tip displacement and twist for wings with ribs orientation of 30°, 40° and 45° is reduced from

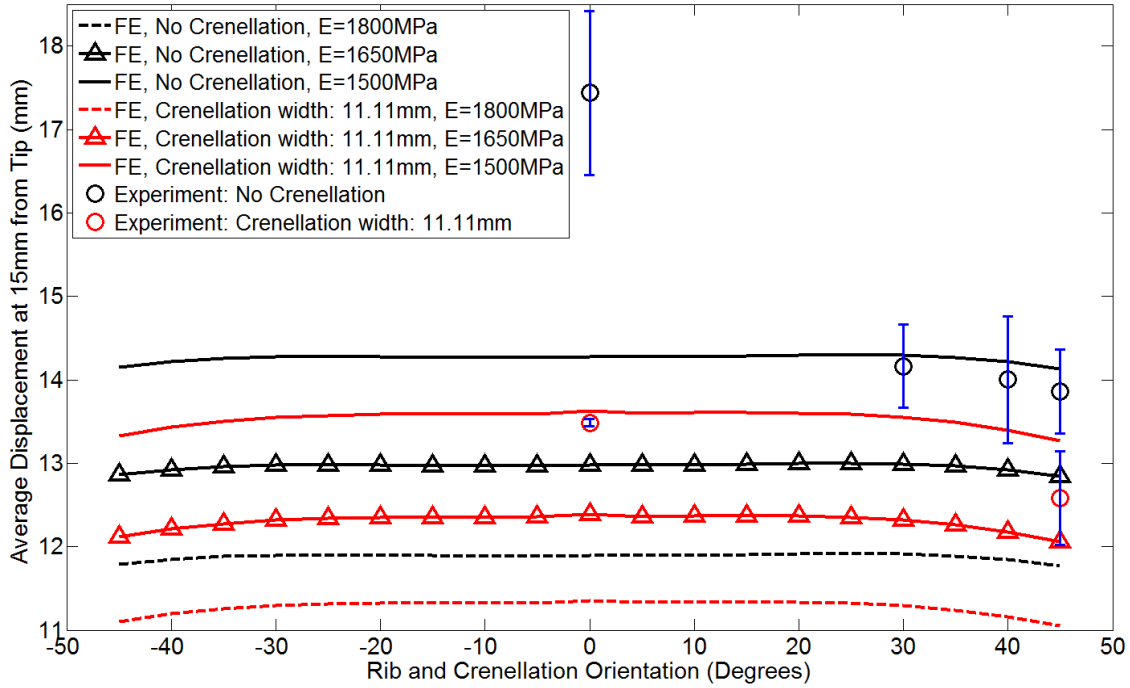

Fig. 14 FE and experimental average displacement at 15 mm from the tip for NACA profiled Wing Box (NWB) with no crenellation and crenellation (width: 11.11 mm)

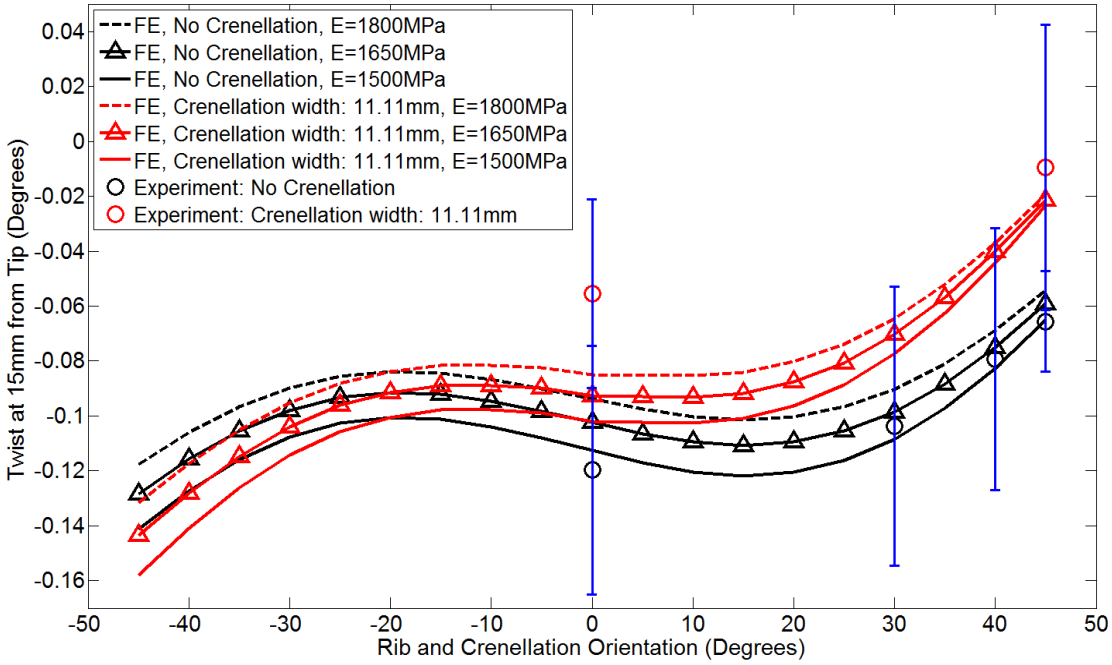

Fig. 15 FE and experimental twist at 15 mm from the tip for NACA profiled Wing Box (NWB) with no crenellation and crenellation (width: 11.11 mm)

9.0% and 10.7% to -1.9% and -4.4% respectively when reducing the tensile modulus from 1,650 MPa to 1,500 MPa. It is believed that the larger errors seen in Fig. 14 and Fig. 15 are the result of manufacturing variability and material property variability. For example, in the experiment the wing with rib/crenellation at 45° displayed a positive twist when loaded. FE results predicted that this wing would have a nose-down twist under load. Further work is investigating those effects.

5.2 Flexural axis

Fig. 16 shows the location of the flexural axis, found using FE modelling, for three rectangular wing boxes with crenellation of width of 11.11 mm: a 0°, -45° and 45° rib/crenellation orientation wing box. It is clear that a positive increase in the rib/crenellation orientation moves the flexural axis backwards. This behaviour explains the increase in nose up tip twist under a mid-chord tip load pulling the wing out of the plane observed in Fig. 11. The conclusion is reversed when considering a negative rib/crenellation orientation.

5.3 Aeroelastic analysis

Fig. 17 and Fig. 18 present the average tip displacement and tip twist for various rectangular box wing designs with and without crenellations of different width and rib/crenellation orientations when subject to aerodynamic loading. Fig. 19 and Fig. 20 show the average tip displacement and tip twist for rectangular wing box designs of different crenellation thickness. These curves display similar trends to the ones presented in the static analysis except that the

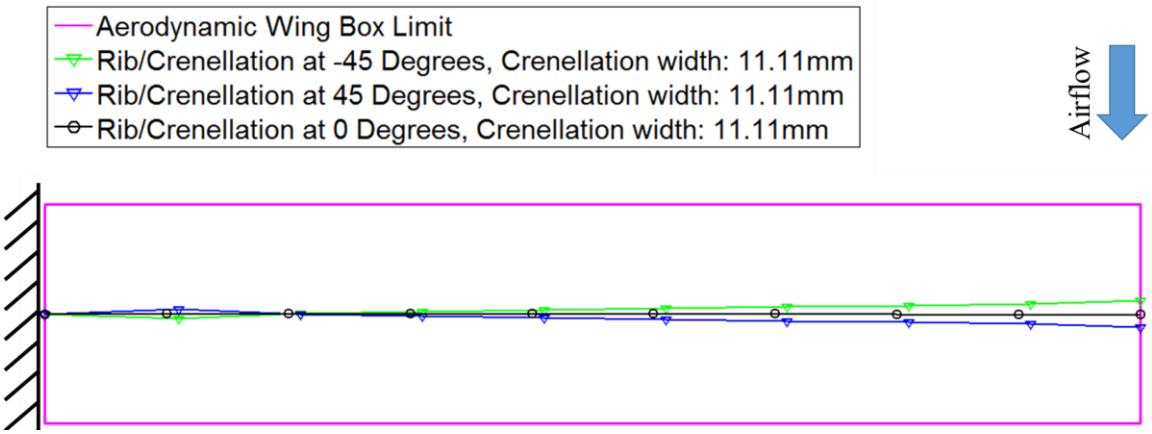

Fig. 16 Flexural axis position for a rectangular wing box with rib/crenellation at -45°, 45° and 0°

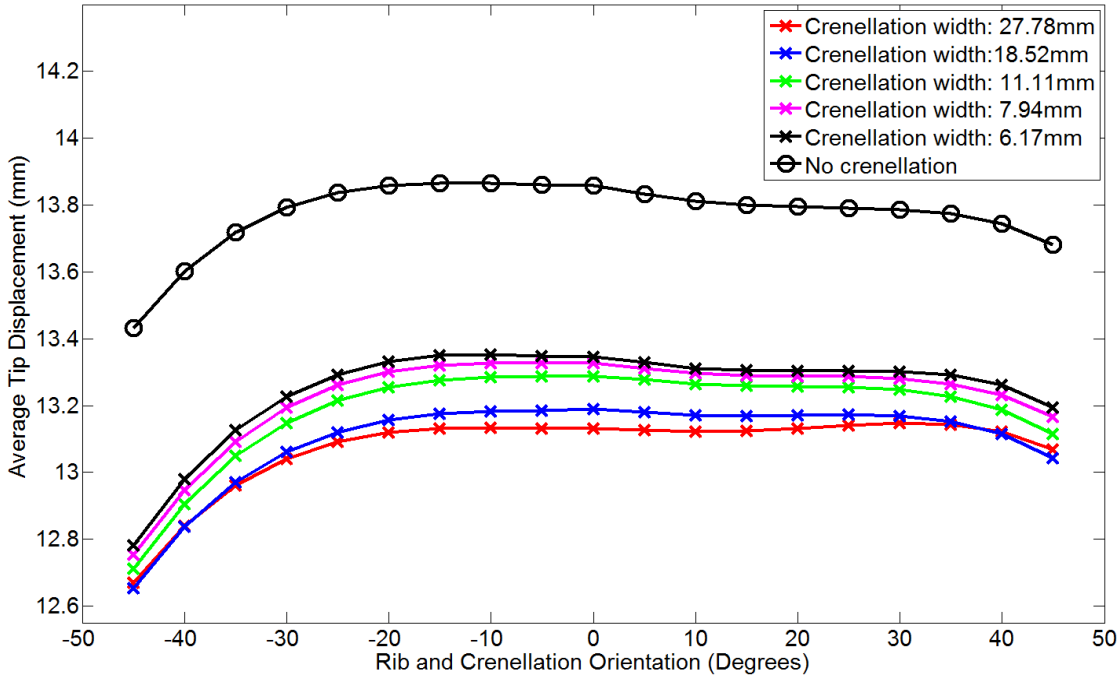

Fig. 17 Average tip displacement for different crenellations width and rib/crenellation orientation on a Rectangular Wing Box (RWB) at an angle of attack of 5° and airspeed of 35 m/s

symmetry found by the 0° rib/crenellation orientation is suppressed.

The addition of crenellations, increasing the crenellation width and its thickness reduce the tip displacement and the nose up tip twist compared to the wing with no crenellation. Changing the rib/crenellation orientation leads to a reduction in tip displacement and a variation in nose up tip twist.

All wings experienced a nose-up tip twist and all the curves' trends seen on Fig. 17-20 are

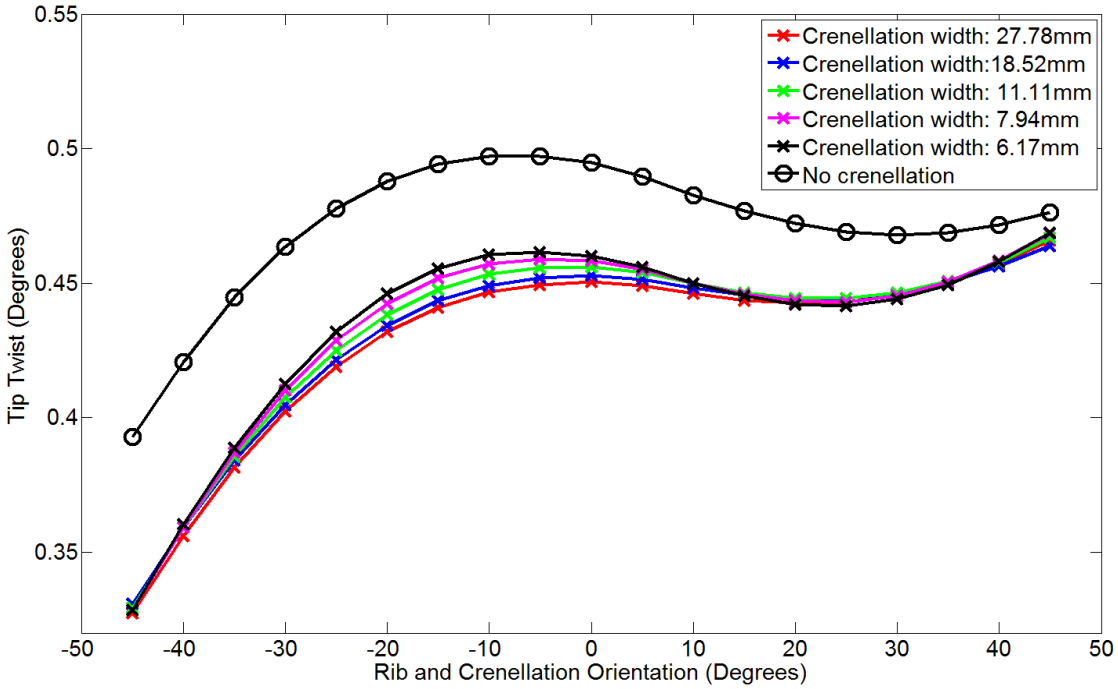

Fig. 18 Tip twist for different crenellations width and rib/crenellation orientation on a Rectangular Wing Box (RWB) at an angle of attack of 5° and airspeed of 35 m/s

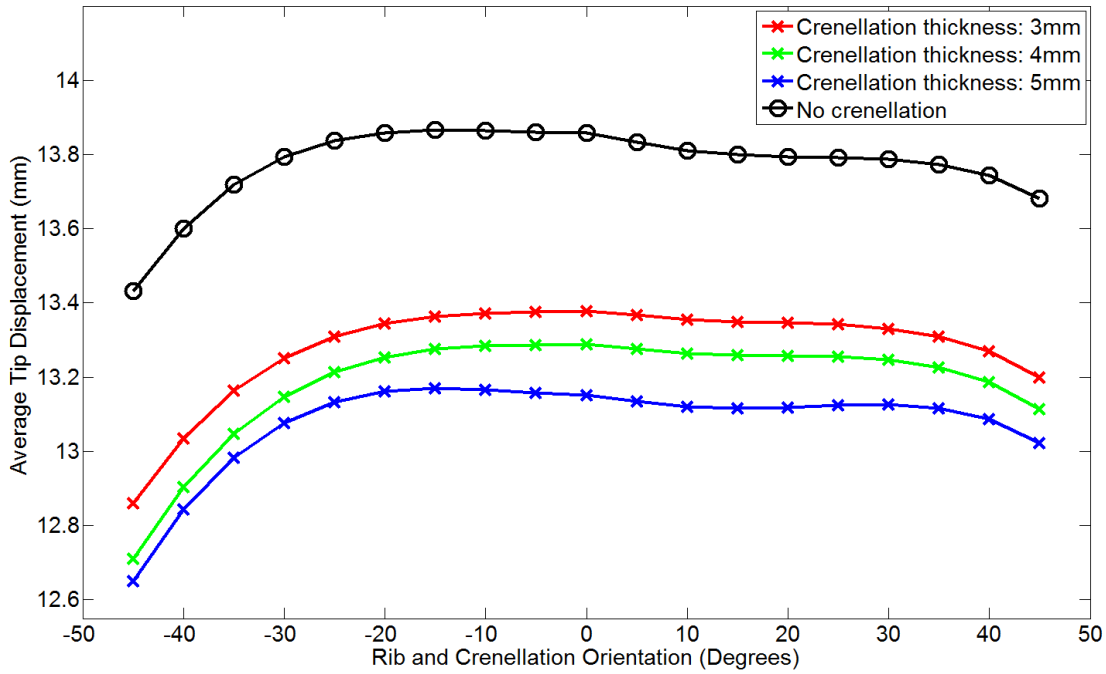

Fig. 19 Average tip displacement for different crenellations thickness and rib/crenellation orientation on a Rectangular Wing Box (RWB) at an angle of attack of 5° and airspeed of 35 m/s

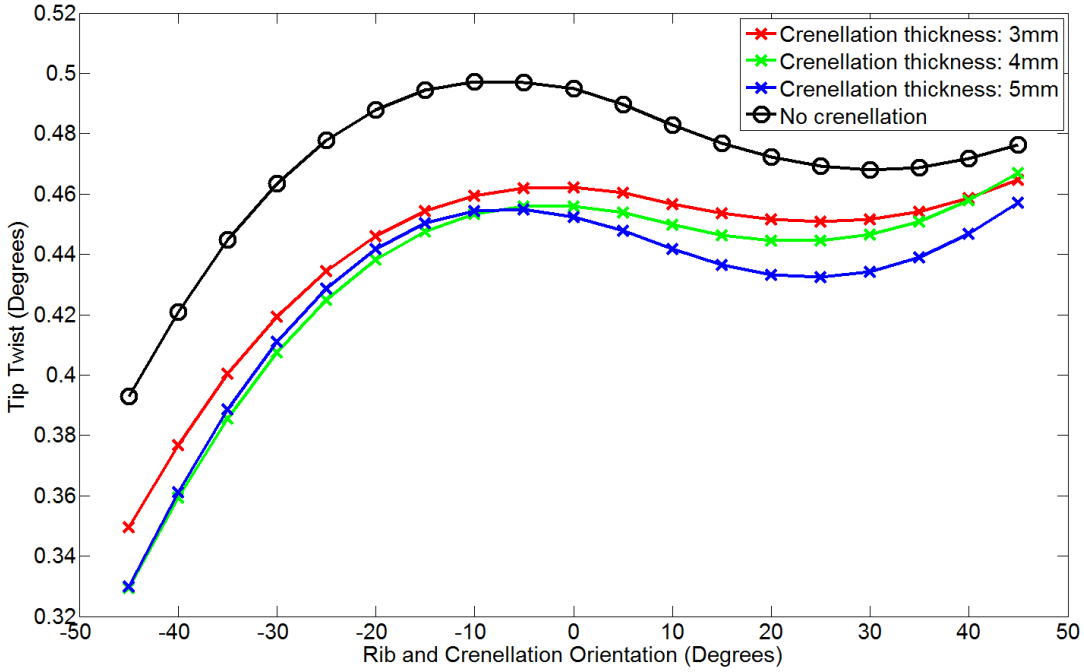

Fig. 20 Tip twist for different crenellations thickness and rib/crenellation orientation on a Rectangular Wing Box (RWB) at an angle of attack of 5° and airspeed of 35 m/s

reduced on the positive rib/crenellation orientation side compared to the curve variation seen in the static load case. The curves' trends are increased in the negative rib/crenellation orientation side.

The nose up tip twist experienced by all wings was expected as in this analysis a span-wise distributed load located around the quarter chord region is used. The movement of the load from the mid-chord position to the quarter chord region means that the load is always located in front of the flexural axis for every wing considered and so a nose-up twist appears.

The lack of symmetry by the 0° rib/crenellation orientation was expected as in this analysis the load varies with the twist distribution produced by the different wings under load. The movement of the load from the mid-chord position to the quarter chord region means that the load is applied closer to the wing flexural axis for wings with a high negative rib/crenellation orientation. Hence, the aerodynamic load produces less torque on such wings, and so less nose-up twist and so less load than the wings with a high positive rib/crenellation orientation.

Fig. 21 and Fig. 22 show the average tip displacement and tip twist for NACA profiled wings with no crenellation and with crenellation of width 11.11 mm with different rib/crenellation orientations when subject to aerodynamic loading. Both FE and experimental results are presented. The FE analysis was performed with three different tensile moduli assuming an elastic material. The experimental results for each wing presented are the average of three wind tunnel runs and the standard deviation for the experimental data is shown as error bars.

The FE results show that the use of a NACA profiled wing removed the symmetry in the tip displacement curve around the 0° rib/crenellation orientation, as previously shown. The addition of a load at the quarter chord magnifies this lack of symmetry. The addition of the crenellation reduces the tip displacement of the wings. The ordinate distance between the two stationary points

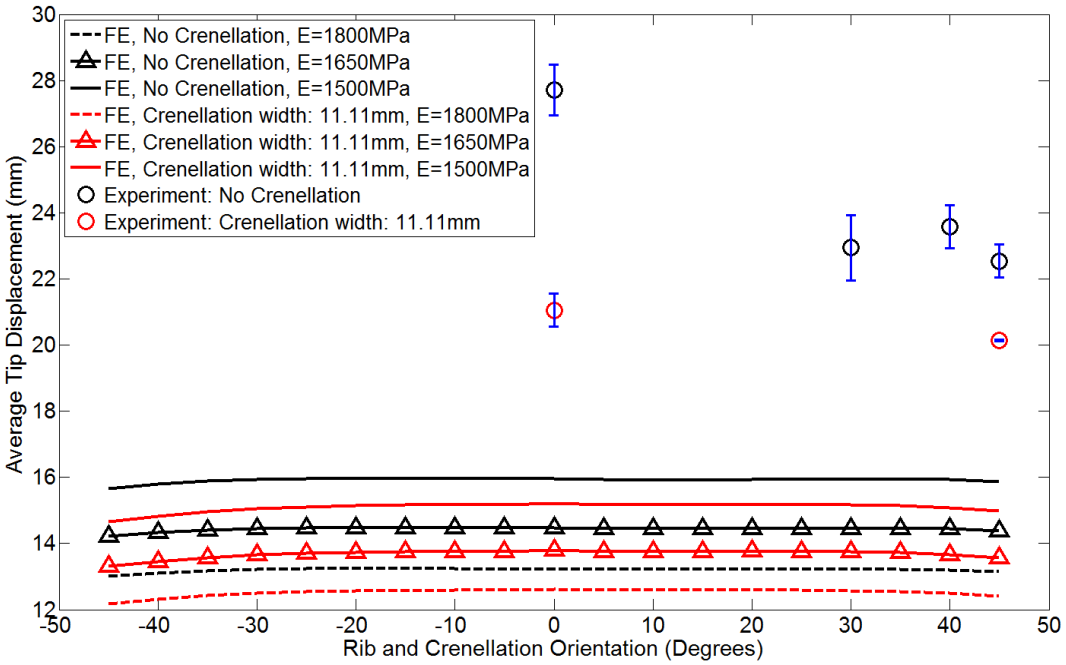

Fig. 21 FE and experimental average tip displacement for NACA profiled Wing Box (NWB) with no crenellation and crenellation (width: 11.11 mm) at an angle of attack of 5° and airspeed of 35 m/s. The experimental results are the average of three wind tunnel runs per wing

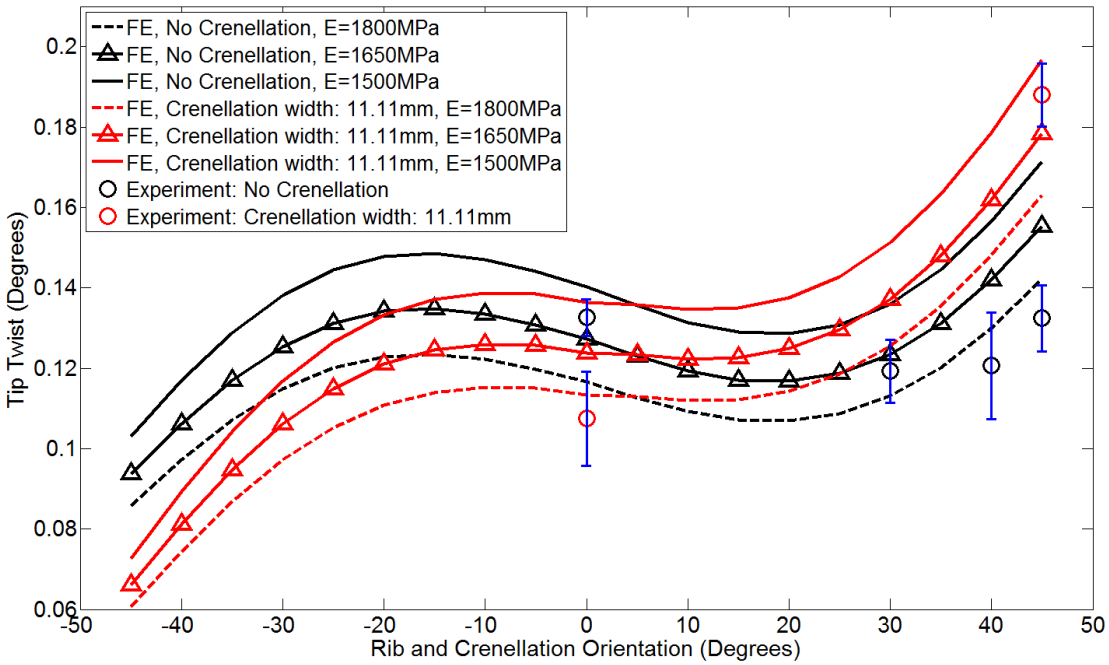

Fig. 22 FE and experimental tip twist for NACA profiled Wing Box (NWB) with no crenellation and crenellation (width: 11.11 mm) at an angle of attack of 5° and airspeed of 35 m/s. The experimental results are the average of three wind tunnel runs per wing

of the cubic tip twist curve is found to reduce and at high rib/crenellation orientation the wing twist is increased by the presence of crenellation.

When considering the experimental results, the major trends of positively increasing the rib/crenellation orientations are respected: a reduction in tip displacement and an increase in positive tip twist. For example the addition of crenellation for wings with ribs at an orientation of 45° reduced the average tip displacement by 10.7% and 5.6% for experimental and FE results respectively and increased the positive tip twist by 41.9% and 14.8%. These variations between FE and experimental results can be explained by the material property variability shown in Section 3.

The tip twist values predicted by FE and the experimental values show a good level of accordance with a maximum difference of -15.1% (E=1,650 MPa). However the difference between tip displacement values predicted by the FE results and the experiment results are much higher (91.6% in the case of the wing with rib at 0° assuming E=1,650 MPa). This variation is larger than the difference observed between FE and experimental results in the static tip load case. This behaviour can be explained due to several factors. First, as shown in Section 3 the material used in the experiment had a viscoelastic behaviour but it was modelled as being elastic in the FE analysis. The viscoelastic behaviour of the wing was appropriately captured in the static experiment by reducing the tensile modulus but this approach is failing in the wind tunnel experiment as the load is deformation dependent. In the wind tunnel experiment the load is dependent of the wing twist deformation hence any additional twist deformation due to stress relaxation and load history leads to higher loads and so higher tip deflection and twist. Additionally, the wind tunnel experiment introduces larger sources of errors through, for example, the angle of attack setting, the impact of any pre-twist created by warping of the wing during the manufacturing process, the control of the temperature in the wind tunnel and the aerofoil's surface finish in addition to the manufacturing and material property variability discussed in Section 5.1.

5.4 Modal analysis

Fig. 23 and Fig. 24 show the variation in the first four natural frequencies of the rectangular wing box model with different crenellation widths and thicknesses. The first four modes are: first bending, second bending, forward/aft and first torsion for all the wings considered except for eight wings. These wings have a rib orientation of ±45° and ±40°. Four wings have a crenellation width of 18.52 mm and four have a crenellation thickness of 3 mm. For those wings the order of the forward/aft and second bending mode swaps. The addition of crenellations, the increase in the number of crenellations and the increase in the crenellation thickness reduce the first three natural frequency of the wing and increase the fourth mode natural frequency highlighting the potential of crenellated skins for flutter control.

It should be noted the wings with crenellation width of 27.78 mm display significantly different natural frequency values for the first three modes compared to other wings with crenellations. This result can be related to the offseted center of gravity towards the tip for that crenellation concept as the first and last rib bay have the same crenelated skin with only one crenellation and one normal skin region. Additionally, this crenellation width was found to introduce the least increase in mass.

Table 6 presents natural frequency data, damping and mode shapes for the first six modes found through modelling and experiment. It should be noted that both the FE and experiment agree on the succession of mode shape with the only exception a forward/aft mode (for./aft) which the experiment could not determine due to the position of the accelerometer.

To compare the agreement between the FE and modelling results Table 7 shows the percentage

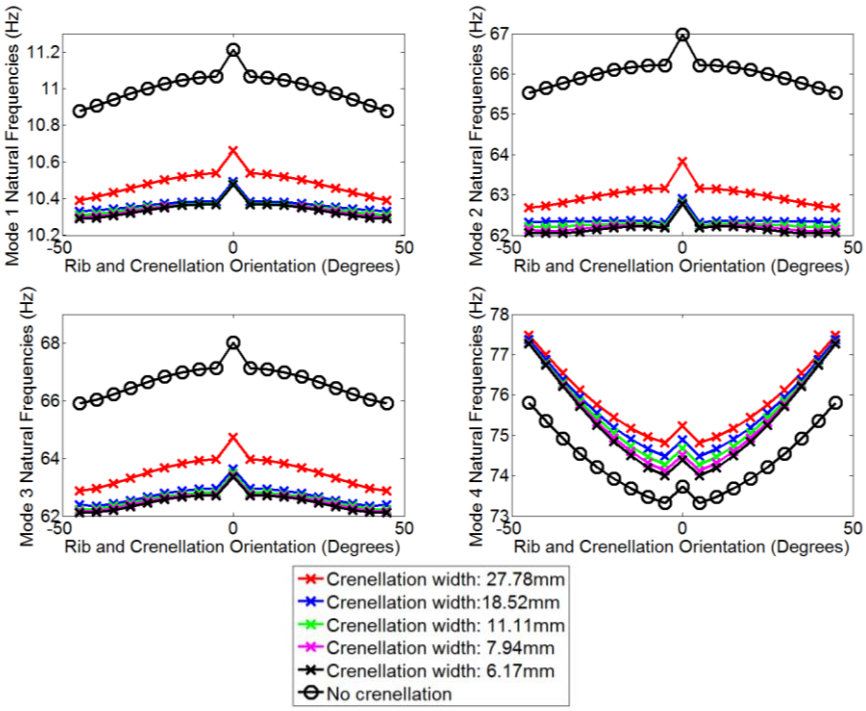

Fig. 23 Variation of the first four natural frequency for wings with no crenellation and crenellation of different width and different rib/crenellation orientation on a Rectangular Wing Box (RWB)

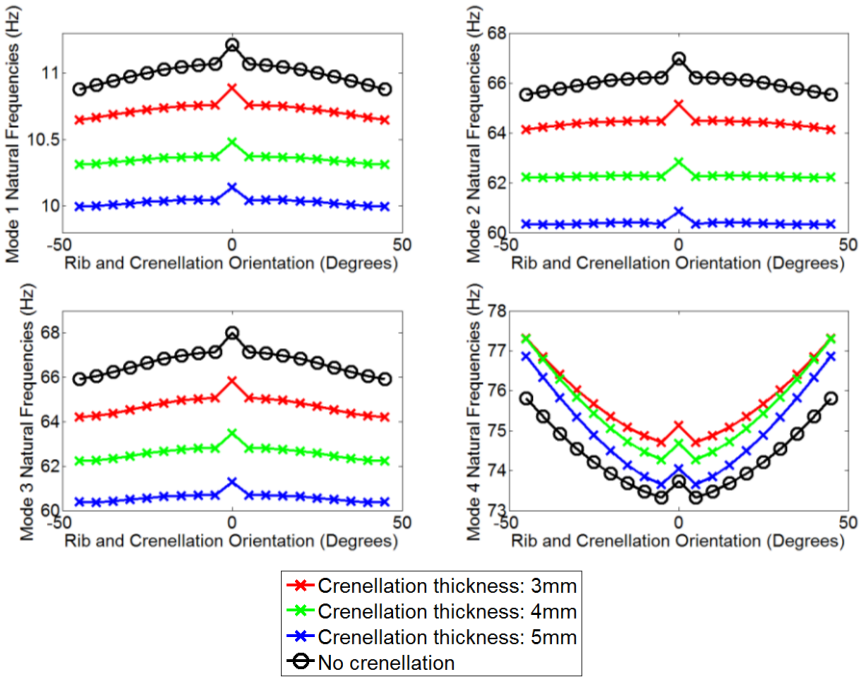

Fig. 24 Variation of the first four natural frequency for wings with no crenellation and crenellation of different thickness and different rib/crenellation orientation on a Rectangular Wing Box (RWB)

Table 6 Experiment and modelling natural frequency, damping and shape results of the first five mode shape for the six wings manufactured

	Ribs @ 0° (R0), No Crenellation					Ribs/ Crenellation @ 0° (R/C0), With Crenellation				
	Experiment			FE		Experiment			FE	
Mode	Freq. (Hz)	Damping %	Shape	Freq. (Hz)	Shape	Freq. (Hz)	Damping %	Shape	Freq. (Hz)	Shape
1	10.63	1.93	Bending	10.74	Bending	10.86	1.27	Bending	10.14	Bending
2	67.51	0.85	Bending	64.63	Bending	68.15	0.85	Bending	61.22	Bending
			For. /Aft	69.52	For. /Aft			For. /Aft	65.16	For. /Aft
3	107.05	0.94	Torsion	96.06	Torsion	114.06	0.86	Torsion	96.76	Torsion
4	186.06	1.23	Bending	171.62	Bending	187.65	0.69	Bending	163.16	Bending
5	321.03	1.05	Torsion	287.66	Torsion	340.37	0.64	Torsion	290.07	Torsion
6	355.28	0.95	Bending	312.47	Bending	354.23	0.88	Bending	298.84	Bending
	Ribs @ 30° (R30), No Crenellation					Ribs @ 40° (R40), No Crenellation				
	Experiment			FE		Experiment			FE	
Mode	Freq. (Hz)	Damping %	Shape	Freq. (Hz)	Shape	Freq. (Hz)	Damping %	Shape	Freq. (Hz)	Shape
1	11.60	0.95	Bending	10.52	Bending	11.54	0.89	Bending	10.48	Bending
2	70.94	1.01	Bending	63.57	Bending	71.19	0.81	Bending	63.44	Bending
			For. /Aft	68.05	For. /Aft			For. /Aft	67.79	For. /Aft
3	114.90	1.06	Torsion	96.69	Torsion	116.33	1.16	Torsion	96.96	Torsion
4	194.20	0.75	Bending	169.70	Bending	194.89	0.77	Bending	169.66	Bending
5	337.02	0.90	Torsion	289.14	Torsion	342.04	0.93	Torsion	289.85	Torsion
6	365.17	0.78	Bending	310.88	Bending	366.68	0.79	Bending	311.44	Bending
	Ribs @ 45° (R45), No Crenellation					Ribs/ Crenellation @ 45° (R/C45), With Crenellation				
	Experiment			FE		Experiment			FE	
Mode	Freq. (Hz)	Damping %	Shape	Freq. (Hz)	Shape	Freq. (Hz)	Damping %	Shape	Freq. (Hz)	Shape
1	11.29	1.18	Bending	10.46	Bending	11.16	0.81	Bending	10.00	Bending
2	70.88	0.78	Bending	63.40	Bending	69.51	0.69	Bending	60.70	Bending
			For. Aft	67.73	For. /Aft			For. /Aft	63.78	Forward/ Aft
3	114.37	1.05	Torsion	96.99	Torsion	118.76	1.05	Torsion	98.31	Torsion
4	194.72	0.74	Bending	169.73	Bending	191.17	0.68	Bending	162.80	Bending
5	343.52	0.82	Torsion	289.87	Torsion	350.80	0.92	Torsion	292.98	Torsion
6	364.88	0.92	Bending	311.97	Bending	363.20	0.94	Bending	300.40	Bending

difference in natural frequencies between the two types of results. The comparison is acceptable with a maximum of 14.5% difference for mode 1 and 2 and a maximum difference of 20.9% for mode 3, 4, 5 and 6.

Finally, Table 8 and Table 9 presents the difference in natural frequency between a wing with

Table 7 Percentage difference in natural frequencies for the first six mode shape between modelling and FE results

	% Difference Between Experiment and FE					
Mode	R0	R/C0	R30	R40	R45	R/C45
1	-1.0	7.1	10.3	10.1	7.9	11.6
2	4.5	11.3	11.6	12.2	11.8	14.5
	100.0	100.0	100.0	100.0	100.0	100.0
3	11.4	17.9	18.8	20.0	17.9	20.8
4	8.4	15.0	14.4	14.9	14.7	17.4
5	11.6	17.3	16.6	18.0	18.5	19.3
6	13.7	18.5	17.5	17.7	17.0	20.9

Table 8 Experimental natural frequencies percentage difference between a wing with no crenellations and wings with varying rib/crenellation orientation

	% Difference with respect to R0, No Crenellation - Experiment				
Mode	R/C0	R30	R40	R45	R/C45
1	2.2	9.1	8.6	6.2	5.0
2	0.9	5.1	5.4	5.0	3.0
3	6.5	7.3	8.7	6.8	10.9
4	0.9	4.4	4.7	4.7	2.7
5	6.0	5.0	6.5	7.0	9.3
6	-0.3	2.8	3.2	2.7	2.2

Table 9 Finite Element natural frequencies percentage difference between a wing with no crenellations and wings with varying rib/crenellation orientation

	% Difference with respect to R0, No Crenellation - FE				
Mode	R/C0	R30	R40	R45	R/C45
1	-5.5	-2.0	-2.4	-2.6	-6.9
2	-5.3	-1.6	-1.8	-1.9	-6.1
	-6.3	-2.1	-2.5	-2.6	-8.2
3	0.7	0.7	0.9	1.0	2.3
4	-4.9	-1.1	-1.1	-1.1	-5.1
5	0.8	0.5	0.8	0.8	2.2
6	-4.4	-0.5	-0.3	-0.2	-3.9

no crenellations, ribs at 0° orientations and with the other wings considered. Both experimental and FE results are used. Clearly both set of results proved that by adding crenellations and changing the orientation of the rib/crenellation one can change the natural frequencies of the wing. It is interesting to note that although the addition of crenellation adds mass to the wing as shown in Table 5 the change in rib/crenellation orientation has a larger impact on the natural frequencies.

5.5 Gust analysis

Fig. 25 and Fig. 26 show the maximum root bending moment encounter by a rectangular wing box model during a gust event with different rib/crenellation orientations and different crenellation widths and thicknesses. Varying the rib and crenellation orientation has a large impact on the maximum root bending moment encountered during a gust event. At high rib/crenellation orientation, the bending moment is shown to reduce by up to 6.4%. This effect can be explained by the reduction in the tip twist values under a static aerodynamic loading as shown by Fig. 18 and Fig. 20. Clearly, the addition of crenellations reduces the maximum root bending moment during a gust encounter, via a reduction in tip twist.

Interestingly Fig. 25 and Fig. 26 show that an optimum solution for the thickness and width of the crenellation must exist to maximize the root bending moment reduction as the wing with the widest crenellation in Fig. 25 and the thickest crenellation in Fig. 26 do not necessarily give the lowest root bending moment for a given rib/crenellation orientation.

It should be noted that although the reduction in tip twist is the dominant reason for the reduction in root bending moment such a metric is also impacted by the variation of the natural frequencies and the variation in wing mass. For example, in Fig. 25 the highest root bending moment value at any rib/crenellation orientation for wings with crenellations is experienced by the wings with the widest crenellations. Interestingly this wing design is the only one that has significantly different first four natural frequency values from the other wing designs with crenellations. Its natural frequencies are the closest to the natural frequencies of wings without crenellations. Additionally this crenellation width was found to introduce the least increase in mass.

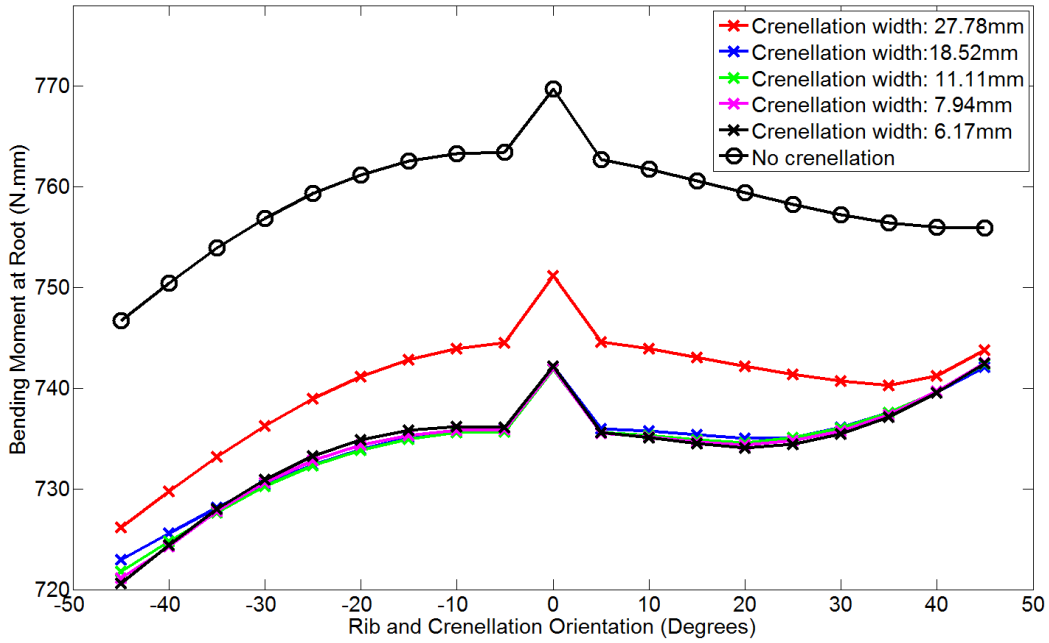

Fig. 25 Maximum bending moment at wing root for different crenellations width and rib/crenellation orientation on a Rectangular Wing Box (RWB) during a gust encounter at an airspeed of 35 m/s

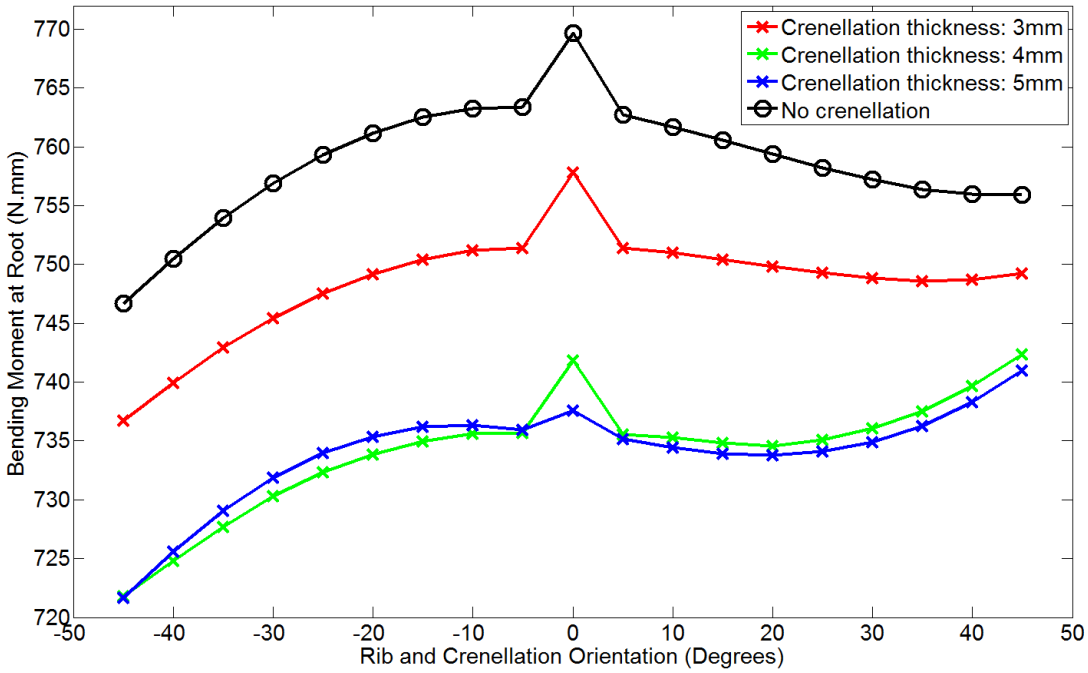

Fig. 26 Maximum bending moment at wing root for different crenellations thickness and rib/crenellation orientation on a Rectangular Wing Box (RWB) during a gust encounter at an airspeed of 35 m/s

5.6 Aeroelastic instability speed analysis

Fig. 27 and Fig. 28 show the first aeroelastic instability speed for a rectangular wing box model with different rib/crenellation orientations and different crenellation widths and thicknesses. All wings are subject to the same first two aeroelastic instabilities: (1) a flutter instability with a coalescence of the first bending mode (dominant), second bending mode and the first torsion mode; and (2) a first bending mode divergence instability. The first aeroelastic instability is due to flutter in all cases except for wings with rib/crenellation at +45° with crenellation width of 11.11, 7.94 and 6.17 mm. These wings undergo divergence first. Hence, the first aeroelastic instability speed is referred to as the flutter/divergence speed.

The variation of the rib orientation has a clear impact on the flutter/divergence speed. The variation of the rib orientation from the -5° orientation increases the flutter/divergence speed by up to 7.5%. The lowest and highest flutter/divergence speed for a wing with no crenellation is 116.8 m/s and 125.6 m/s for wings with rib orientation of -5° and -45° respectively. The lack of symmetry by the 0° orientation can be related to the lack of symmetry in the aerodynamic loading as explained in Section 5.3.

The addition of crenellation at any rib/crenellation orientation increases the flutter/divergence speed when compared to wings with no crenellation of similar rib orientation. For example, at a rib/crenellation orientation of 0° adding crenellation increases the flutter/divergence speed by at least 3.9%. It should be noted that such a wing does not display any bend-twist coupling hence the increase in first aeroelastic instability speed was due to an increase in wing stiffness and wing mass. However when the rib/crenellation orientation is different than 0°, the increase in

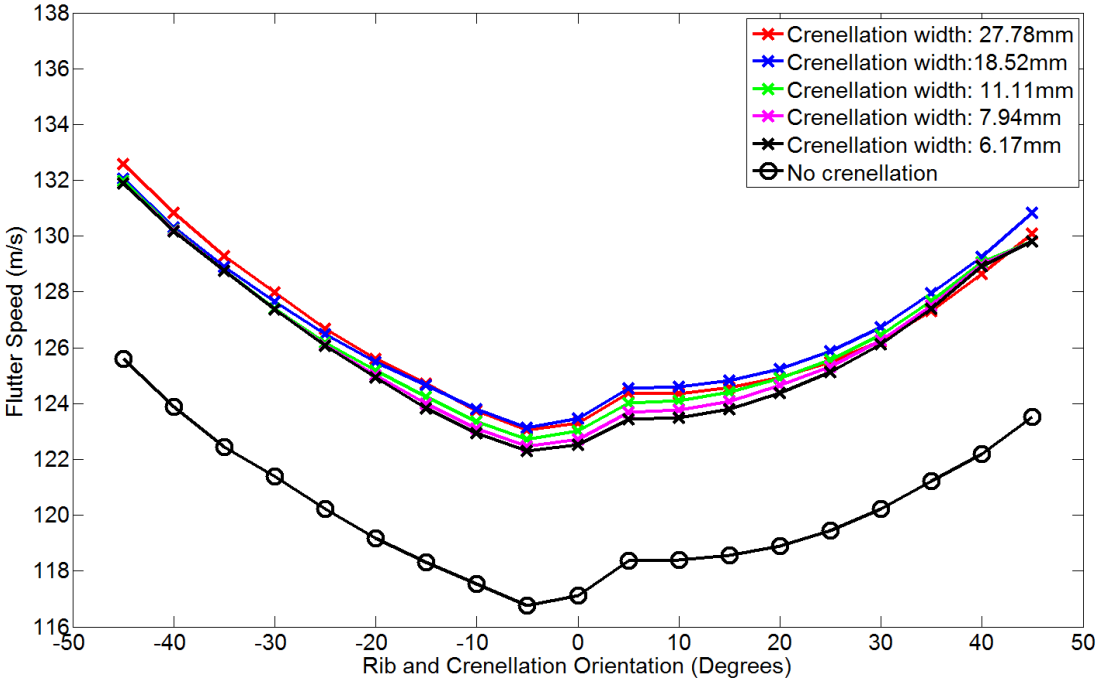

Fig. 27 First aeroelastic instability speed for different crenellations width and rib/crenellation orientation on a Rectangular Wing Box (RWB)

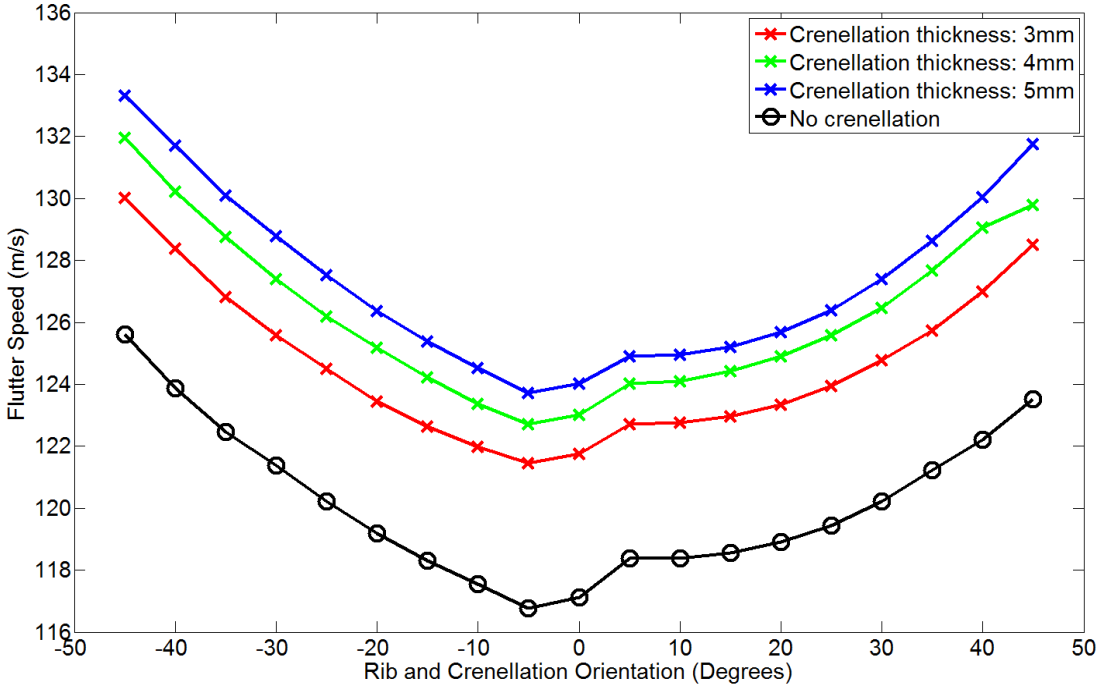

Fig. 28 First aeroelastic instability speed for different crenellations thickness and rib/crenellation orientation on a Rectangular Wing Box (RWB)

flutter/divergence speed is also due to a change in wing bend-twist coupling.

The increase in crenellation width has overall a very small effect on the flutter speed compared to adding crenellation with a maximum increase in flutter/divergence speed of 0.8% compared to the thinnest crenellation considered. Increasing the crenellation thicknesses increases the flutter speed. When varying the crenellation orientation from 3 mm to 5 mm the flutter speed was found to increase by at least 1.8% in every rib/crenellation orientation considered.

6. Conclusions

The effect of a crenellated skin was explored to control the aeroelastic performance of a wing. The rib/crenellation orientation, the crenellation width and thickness were used to control the tip displacement, tip twist and the wing's natural frequencies. The wings were subjected to various static and aerodynamic loads through FE modelling and experiments. Finally, the impact of crenellations on the maximum root bending moment encounter during a gust event and the first aeroelastic instability speed was investigated. It was shown that the rib orientation changed the wing bend-twist coupling and this variation can be increased by the crenellated skin concept. This leads to a maximum increase in flutter/divergence speed by 14.2% and gust loads alleviation by 6.4% using the rib/crenellations orientations.

The FE results clearly proved that the crenellated skin can affect wing deformation under load. Additionally, the coupling of the crenellation and rib orientation offered extra control on the wing deformation. The experiments validated the increase in stiffness linked with the crenellated skin and the increase in rib/crenellation orientation. However, some significant difference was recorded between the FE and experimental results in the aeroelastic experiment. This effect is still being investigated but is strongly affected by the consistency and quality of the manufacturing technique (3D printing) and materials used. Future work will consider the use of viscoelastic material properties in the FE analyses to introduce stress relaxation and load history.

Acknowledgments

The authors gratefully acknowledged the support of the EPRSC under its ACCIS Centre for Doctoral Training grant, EP/G036772/1, the Royal Academy of Engineering and the European Office of Aerospace and Development. The authors would also like to thank Julian Londono for his help with the LMS International software. Part of this work was carried out using the computational facilities of the Advanced Computing Research Centre, University of Bristol - http://www.bris.ac.uk/acrc/.

References

Airbus (2013), "Future Journeys 2013-2032", Retrieved May 8, 2015 (http://www.airbus.com/company/market/forecast/?eID=dam_frontend_push&docID=33752.

Bendsøe, M.P. and Sigmund, O. (2003), *Topology Optimization Theory, Methods and Applications*, Springer.

Brampton, C.J., Kim, H.A. and Cunningham, J.L. (2012), "Level set topology optimisation of aircraft wing considering aerostructural interaction", *12th AIAA Aviation Technology, Integration, and Operations*

(ATIO) Conference and 14th AIAA/ISSM, Indianapolis, Indiana, U.S.A., September.
Dunning, P.D., Stanford, B.K. and Kim, H.A. (2014), "Aerostructural level set topology optimization for a common research model wing", *10th AIAA Multidisciplinary Design Optimization Conference*, National Harbor, Maryland, U.S.A., January.
Dunning, P.D., Stanford, B.K. and Kim, H.A. (2015), "Level-set topology optimization with aeroelastic constraints", *56th AIAA/ASMe/ASCE/AHS/SC Structures, Structural Dynamics, and Material Conference*, Kissimmee, Florida, U.S.A., January.
Eastep, F.E., Tischler, V.A., Venkayya, V.B. and Khot, N.S. (1999), "Aeroelastic tailoring of composite structures", *J. Aircraft*, **36**(6), 1041-47.
European Aviation Safety Agency (2013), *Certification Specifications for Normal, Utility, Aerobatic, and Commuter Catergory Aeroplanes CS 23*.
Francois, G. and Cooper, J.E. (2014), "Novel structural wing designs for forward swept wings", *2014 Royal Aeronautical Society Biennial Applied Aerodynamics Research Conference*, Bristol ,U.K., July.
Francois, G., Cooper, J.E. and Weaver, P.M. (2014) "Aeroelastic tailoring of composite wings using internal structural members shape and stacking sequence", *4th Aircraft Structural Design Conference*, Belfast, U.K., October.
Francois, G., Cooper, J.E. and Weaver, P.M. (2015), "Aeroelastic tailoring using rib/spar orientations: experimental investigation", *56th AIAA/ASMe/ASCE/AHS/SC Structures, Structural Dynamics, and Material Conference*, Kissimmee, Florida, U.S.A., January.
Guo, S. (2007), "Aeroelastic optimization of an aerobatic aircraft wing structure", *Aerosp. Sci. Technol.*, **11**(5), 396-404.
Guo, S., Li, D. and Liu, Y. (2011), "Multi-objective optimization of a composite wing subject to strength and aeroelastic constraints", *Proceedings of the Institution of Mechanical Engineers, Part G: Journal of Aerospace Engineering*, **226**(9), 1095-1106.
Harmin, M.Y., Ahmed, A.T., Cooper, J.E. and Bron, F. (2011), "Aeroelastic tailoring of metallic wing structures", *52nd AIAA/ASME/ASCE/AHS/ASC Structures, Structural Dynamics and Materials Conference*, Denver, Colorado, U.S.A., April.
Imetrum (2016), Retrieved February 1, (http://www.imetrum.com/).
Johnson, E.H. (1997), "MSC developments in aeroelasticity", *1997 MSC Aerospace Users' Conference*.
Jutte, C.V., Stanford, B.K., Wieseman, C.D. and Moore, J.B. (2014), "Aeroelastic tailoring of the NASA common research model via novel material and structural configurations", *53th AIAA/ASMe/ASCE/ AHS/SC Structures, Structural Dynamics, and Material Conference*, National Harbor, Maryland, U.S.A., January.
Kim, T. and Hwang, I.H. (2005), "Optimal design of composite wing subjected to gust loads", *Comput. Struct.*, **83**(19-20), 1546-54.
Kolonay, R.M. and Kobayashi, M.H. (2010), "Topology, shape, and sizing optimization of aircraft lifting surfaces using a cellular division method", *13th AIAA/ISSMO Multidisciplinary Analysis Optimization Conference*, Forth Worth, Texas, U.S.A., September.
Liu, Q., Jrad, M., Mulani, S.B. and Kapania, R.K. (2015), "Integrated global wing and local panel optimization of aircraft wing", *56th AIAA/ASMe/ASCE/AHS/SC Structures, Structural Dynamics, and Material Conference*, Kissimmee, Florida, U.S.A., Janurary.
Liu, Q., Mulani, S. and Kapania, R.K. (2014), "Global/local multidisciplinary design optimization of subsonic wing", *53th AIAA/ASMe/ASCE/AHS/SC Structures, Structural Dynamics, and Material Conference*, National Harbor, Maryland, U.S.A, January.
Locatelli, D., Mulani, S.B. and Kapania, R.K. (2011), "Wing-box weight optimization using curvilinear spars and ribs (SpaRibs)", *J. Aircraft*, **48**(5), 1671-84.
Manan, A., Vio, G.A., Harmin, M.Y. and Cooper, J.E. (2010), "Optimization of aeroelastic composite structures using evolutionary algorithms", *Eng. Optim.*, **42**(2), 171-84.
Maute, K. and Allen, M. (2004), "Conceptual design of aeroelastic structures by topology optimization", *Struct. Multidisc. Optim.*, **27**(1-2), 27-42.
Rodden, W.P. and Johnson, E.H. (1994), *MSC/NASTRAN Aeroelastic Analysis User's Guide v68*, The

MacNeal-Schwendler Corporation, Los Angeles, California, U.S.A.

Stanford, B.K., Wieseman, C.D. and Jutte, C.V. (2015), "Aeroelastic tailoring of transport wings including transonic flutter constraints", *56th AIAA/ASMe/ASCE/AHS/SC Structures, Structural Dynamics, and Material Conference*, Kissimmee, Florida, U.S.A., January.

Stodieck, O., Cooper, J.E. and Weaver, P.M. (2015), "On the interpretation of bending-torsion coupling for wwept, non-homogenous wings", *56th AIAA/ASMe/ASCE/AHS/SC Structures, Structural Dynamics, and Material Conference*, Kissimmee, Florida, U.S.A., January.

Stodieck, O., Cooper, J.E., Weaver, P.M. and Kealy, P. (2013), "Improved aeroelastic tailoring using tow-steered composites", *Compos. Struct.*, **106**, 703-15.

Stodieck, O., Cooper, J.E., Weaver, P.M. and Kealy, P. (2014), "Optimisation of tow-steered composite wing laminates for aeroelastic tailoring", *53th AIAA/ASMe/ASCE/AHS/SC Structures, Structural Dynamics, and Material Conference*, National Harbor, Maryland, U.S.A., January.

Tatham, R. (1951), "Shear centre, flexural centre and flexural axis: an attempt to clear up current confusion and provide definitions differentiating between the three terms", *Aircraft Eng. Aerosp. Tech.*, **23**(7), 209-10.

Vio, G.A. and Fitzpatrick, I.R. (2012), "Design of composite structures for improved aeroelastic performance", *28th International Council of the Aeronautical Sciences*, Brisbane, Australia, September.

Vio, G.A., Georgiou, G.and Cooper, J.E. (2012), "Design of composite structures to improve the aeroelastic performance", *53rd AIAA/ASME/ASCE/AHS/ASC Structures, Structural Dynamics and Materials Conference*, Honolulu, Hawai, U.S.A., April.

Weisshaar, T.A. (1981), "Aeroelastic tailoring of forward swept composite wings", *J. Aircraft*, **18**(8), 669-676.

Weisshaar, T.A. (1987), "Aeroelastic tailoring-creative uses of unusual materials", *AIAA/ASME/ASCE /AHS 28th Structures, Structural Dynamics and Materials Conference*, Monterey, California, U.S.A., April.

Wright, J.R. and Cooper, J.E. (2007), *Introduction to Aircraft Aeroelasticity and Loads*, Wiley, Chichester, U.K.